



The Arctic overturning circulation: transformations, pathways and timescales

Jakob Dörr^{1,★}, Carlo Mans^{1,★}, Marius Årthun¹, Kristofer Döös², Dafydd Gwyn Evans³, and Yanchun He⁴

¹Geophysical Institute, University of Bergen and Bjerknes Centre for Climate Research, Bergen, Norway

²Department of Meteorology, Stockholm University, Stockholm, Sweden

³National Oceanography Centre, Southampton, UK

⁴Nansen Environmental and Remote Sensing Center and Bjerknes Centre for Climate Research, Bergen, Norway

★These authors contributed equally to this work.

Correspondence: Jakob Dörr (jakob.dorr@uib.no)

Received: 5 September 2025 – Discussion started: 17 September 2025

Revised: 19 December 2025 – Accepted: 28 January 2026 – Published: 12 February 2026

Abstract. The Arctic is the northernmost terminus of the Atlantic Meridional Overturning Circulation and is an important source of the densest waters feeding its lower limb. However, relatively little is known about the structure and timescales of the Arctic overturning circulation, and which pathways contribute most to the transformation of Atlantic Waters into dense waters and Polar Waters. In this work, we combine a Eulerian water mass transformation framework and Lagrangian tracking to decompose the time-mean Arctic overturning circulation in an eddy-rich (1/12°) global ocean hindcast (1979–2015). We show that the Atlantic Water branch through the Barents Sea dominates dense Arctic overturning, and that a large portion of these transformed waters takes many decades to exit Fram Strait. Furthermore, we show that surface forcing in the Barents Sea and north of Svalbard dominates dense overturning, but local subsurface mixing with shelf waters and between the two Atlantic Water branches plays an important role for the Fram Strait branch. Our work identifies the dominant processes of the Arctic overturning circulation, and can be used as a baseline to understand its future changes and their impact on the stability of Atlantic overturning.

1 Introduction

A key component of the Atlantic Meridional Overturning Circulation (AMOC) is the transformation of Atlantic Waters into dense waters at high latitudes (Buckley et al., 2023). Considerable attention has been directed toward understanding the overturning processes in the subpolar North Atlantic and Nordic Seas, where the production of dense waters supply the lower limb of the AMOC (Dickson and Brown, 1994; Chafik and Rossby, 2019; Petit et al., 2020; Yeager et al., 2021; Årthun, 2023). Recently, it has been recognized that also the Arctic Ocean is a major component in the production of the densest waters sustaining the AMOC (Zhang and Thomas, 2021). However, the understanding of the overturning circulation in the Arctic Ocean is much less developed and a detailed description of overturning processes in the Arctic is lacking.

Warm and salty Atlantic Water enters the Nordic Seas across the Greenland-Scotland Ridge and flows northward along its eastern boundary (Orvik and Niiler, 2002). It then enters the Arctic Ocean as two distinct branches, via the Fram Strait and the Barents Sea opening (Fig. 1; Beszczynska-Möller et al., 2011). Within the Arctic Ocean, the Fram Strait and Barents Sea branches of Atlantic Water merge at St. Anna trough, and continue flowing around the deep Arctic basins as a cyclonic boundary current (Coachman and Barnes, 1963; Timmermans and Marshall, 2020). As the two branches meet, they interact and exchange properties (Schauer et al., 2002). As Atlantic Water circumnav-

igates the Arctic Ocean, it is both cooled and freshened through heat loss to the atmosphere as well as interaction with sea ice and shelf waters (Rudels et al., 2015; Ivanov et al., 2024). A large part of the surface heat loss occurs in the Barents Sea (Skagseth et al., 2020; Smedsrød et al., 2013). As a result, the Barents Sea branch is colder and denser than the Fram Strait branch, and occupies a deeper part of the water column than the Fram Strait branch (Aksenov et al., 2011; Moat et al., 2014). On the Pacific side of the Arctic Ocean, inflowing Pacific Waters undergo comparable modification processes, and serve as an additional source of heat and freshwater (Tsubouchi et al., 2024).

The transformation of these inflowing water masses gives rise to the production of two key outflow products: Dense Waters and Polar Waters (Haine, 2021; Tsubouchi et al., 2024). These outflow types are frequently characterized as resulting from two distinct circulations in a so-called double estuarine representation of the Arctic Ocean circulation (Carmack and Wassmann, 2006; Eldevik and Nilsen, 2013; Haine, 2021; Brown et al., 2025). The thermal overturning branch represents the conversion of Atlantic Water into cooler and slightly fresher waters, resulting in the formation of Dense Water. These dense waters recirculate back to the Nordic Seas through the deep sections of the Fram Strait. In contrast, the estuarine branch represents the gradual freshening and cooling of Atlantic Water through mixing with fresher waters, formed largely through ice melt and river runoff, to produce buoyant Polar Waters, which are exported through outflows in the upper layers of the Davis and Fram Straits (e.g. Rudels et al., 2004).

In a warming climate, the overturning circulation in the North Atlantic (i.e. the AMOC) is projected to decline as the necessary dense water formation is inhibited by warmer and fresher surface waters (Asbjørnsen and Árthun, 2023; Weijer et al., 2020). In contrast, in the Arctic Ocean, sea-ice loss might lead to a stronger surface exposure of Atlantic Water and hence increased dense water formation, potentially stabilizing the northern overturning circulation (Lique and Thomas, 2018; Bretones et al., 2022; Árthun et al., 2025). In order to better project the response of Arctic overturning to future warming, it is important to understand how Atlantic Water entering the Arctic Ocean is transformed before being exported as dense waters to join the lower limb of the the AMOC. Although the general transformation processes required to produce the outflow products are known, the relative contributions of surface forcing and interior mixing are not. It is also not established nor quantified where along the Atlantic Water pathways the transformation is most pronounced, or which processes dominate. While it is known that the Barents Sea branch undergoes the strongest surface heat loss (Skagseth et al., 2020), the relative importance of the two Atlantic Water branches for the thermal branch of Arctic overturning has not been quantified.

In this work, we analyze the mean structure of the Arctic overturning circulation in a global eddy-rich ocean hindcast,

using both an Eulerian water mass transformation framework (Walsh, 1982; Pemberton et al., 2015; Evans et al., 2023) and offline Lagrangian trajectories. We quantify the transformation of Atlantic Water into Polar Water and dense waters, and estimate the relative contribution of surface processes and internal mixing, and their seasonal variability. Furthermore, we quantify the relative importance of the two Atlantic Water branches, and the geographic locations of water mass transformation.

2 Materials and Methods

2.1 NEMO ocean hindcast

For our analysis of the Arctic overturning circulation, we use output from a global NEMO ocean hindcast simulation (ORCA0083-N06; Moat et al., 2016). The simulation is based on NEMO-LIM2 with a horizontal resolution of 1/12°, which is approximately 3–5 km in the Arctic, and 75 unevenly spaced depth layers. The model is forced with atmospheric and river runoff data from the DRAKKAR forcing set 5.2 (Dussin et al., 2018) and was run from 1958 to 2015. To prevent excessive drifts in salinity, sea-surface salinity is relaxed towards climatology (Moat et al., 2016). We consider output from 1979 to 2015 in this study. We make use of the monthly mean velocity and tracer output.

ORCA0083-N06 has previously been used to study the Arctic Ocean, and the upper ocean circulation, sea surface height and mixed-layer depth has been found to match well with observations (Kelly et al., 2018, 2019; Wilson et al., 2021). Furthermore, NEMO has been extensively validated in the Arctic Ocean, and previous and similar versions have found to generally perform well (Lique et al., 2010). Nevertheless, we evaluate the model against observational estimates of net volume transports at the gateways in Table 1. Acknowledging that the observations cover different periods than the model, the net volume transports at the Arctic gateways are generally consistent with observational estimates, although ORCA0083-N06 overestimates the net outflow through Fram Strait and underestimates the outflow through Davis Strait compared to the most recent estimates. However, the inflow of Atlantic water through Fram Strait ($T > 2^{\circ}\text{C}$, $S > 34.7$) for the period 1997–2015 is 3.0 Sv, close to the estimate of 3.0 ± 0.2 Sv by Beszczynska-Möller et al. (2012). The inflow of Atlantic Water ($T > 3^{\circ}\text{C}$) through the Barents Sea Opening between 75–73.5°N is 2.4 Sv, consistent with estimates from mooring data of 2.1 ± 1.0 Sv (Smedsrød et al., 2022). The temperature and depth of the Atlantic Water core in the Arctic Ocean is similar to estimates from the PHC3.0 climatology (Steele et al., 2001), but with a cold bias in the Makarov Basin (Fig. A1). We conduct a more thorough evaluation of the Arctic overturning streamfunction and Atlantic Water pathways below, and show that the hindcast is able to realistically simulate both.

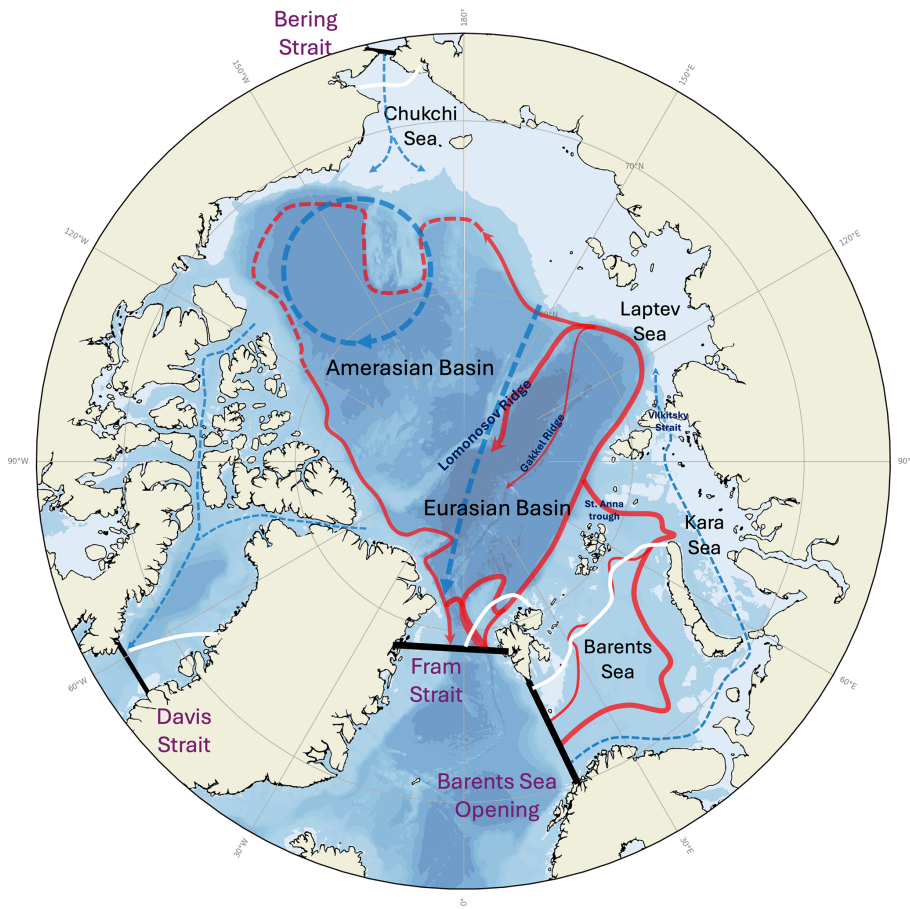


Figure 1. Overview of the Arctic Ocean, including its four oceanic gateways, relevant regional seas, ocean basins and ridges, and a schematic of the major Atlantic Water (red) and surface layer (blue) pathways. White lines denote approximate locations of the annual mean sea-ice edge.

Table 1. Comparison of ocean volume transports from ORCA0083-N06 with observational estimates. Uncertainty values denote the interannual standard deviation over 1979–2015 for the model.

Gateway	ORCA0083-N06 (1979–2015)	Observation-based estimate
Bering Strait	$1.3 \pm 0.5 \text{ Sv}$	$1.0 \pm 0.5 \text{ Sv}$ (Woodgate, 2018)
Barents Sea Opening	$3.5 \pm 1.0 \text{ Sv}$	3.3 Sv (Rudels et al., 2015)
Fram Strait	$-3.0 \pm 0.9 \text{ Sv}$	$-2.0 \pm 2.7 \text{ Sv}$ (Beszczynska-Möller et al., 2011)
Davis Strait	$-1.8 \pm 0.7 \text{ Sv}$	$-2.6 \pm 1.0 \text{ Sv}$ (Curry et al., 2011)

2.2 Water mass transformation framework

2.2.1 Density transformation

Following previous studies (e.g. Pemberton et al., 2015; Evans et al., 2023; Årthun et al., 2025), we use the Walin framework (Walin, 1982) to diagnose the volume budget for the Arctic Ocean in density (σ) and temperature-salinity ($T-S$) space. Here we define the Arctic Ocean domain by its four major gateways: Fram Strait, the Barents Sea Opening, Bering Strait, and Davis Strait (Fig. 1). The volume tendency in a given density class can be expressed as the sum of the

net advective transport across the boundaries of that class and the divergence of water mass transformation within it (Walin, 1982; Buckley et al., 2023; Evans et al., 2023; Zou et al., 2024):

$$\frac{dV_\sigma(\sigma^*, t)}{dt} = M_\sigma(\sigma^*, t) + \frac{\partial G_\sigma(\sigma^*, t)}{\partial \sigma}, \quad (1)$$

where $V_\sigma(\sigma^*, t)$ is the volume of water, $M_\sigma(\sigma^*, t)$ represents the net advective volume transport and $G_\sigma(\sigma^*, t)$ denotes the water mass transformation within a tracer bin centered on density σ_0^* , and bounded by $\sigma_0^* \pm \Delta\sigma/2$. As such, the convergence of the water mass transformation is also referred

to as the water mass formation (WMF), and divergence is referred to as water mass destruction. The water mass transformation processes that affect water with density σ_0^* can be summarized as air-sea buoyancy fluxes where σ_0^* outcrops, and unresolved residual interior mixing processes, such that:

$$G_\sigma(\sigma^*, t) = F_\sigma^{\text{sfc}}(\sigma^*, t) + F_\sigma^{\text{res}}(\sigma^*, t), \quad (2)$$

with $F_\sigma^{\text{sfc}}(\sigma^*, t)$ the surface forced component and $F_\sigma^{\text{res}}(\sigma^*, t)$ the residual.

2.2.2 Temperature-salinity transformation

The volume tendency in a given T - S class can be expressed as the sum of the net advective transport across the boundaries of that class and the divergence of water mass transformation within it:

$$\frac{dV_{S\Theta}(\Theta^*, S^*, t)}{dt} = M_{S\Theta}(\Theta^*, S^*, t) + \frac{\partial G_\Theta(\Theta^*, S, t)}{\partial \Theta} + \frac{\partial G_S(\Theta, S^*, t)}{\partial S}, \quad (3)$$

where $V_{S\Theta}(\Theta^*, S^*, t)$ is the volume of water within a tracer bin centered on temperature Θ^* and salinity S^* , and bounded by $\Theta^* \pm \Delta\Theta/2$ and $S^* \pm \Delta S/2$. $M_{S\Theta}$ represents the net advective transport and G_Θ and G_S denote the water mass transformation in the domain. The net advective transport is defined as:

$$M_{S\Theta}(\Theta^*, S^*, t) = \psi_{S\Theta|\text{Fram}} + \psi_{S\Theta|\text{BSO}} + \psi_{S\Theta|\text{Bering}} + \psi_{S\Theta|\text{Davis}}, \quad (4)$$

where ψ is the net volume transport within a tracer bin along a section and is calculated as

$$\psi_{S\Theta}(\Theta^*, S^*, t) = \iint \Pi[\Theta, \Theta^*] \Pi[S, S^*] v \, dx \, dz.$$

Here, Π is a boxcar function equal to 1 if $\Theta \in [\Theta^* - \Delta\Theta/2, \Theta^* + \Delta\Theta/2]$ (and similarly for salinity), and 0 otherwise, while v is the velocity normal to the section (positive northward). We decompose the water mass transformation terms into separate terms as:

$$G_\Theta(\Theta^*, S, t) = F_\Theta^{\text{sfc}}(\Theta^*, S, t) + F_\Theta^{\text{res}}(\Theta^*, S, t), \\ G_S(\Theta, S^*, t) = F_S^{\text{sfc}}(\Theta, S^*, t) + F_S^{\text{res}}(\Theta, S^*, t), \quad (5)$$

where F_Θ^{sfc} and F_S^{sfc} are referred to as the surface forced transformation. The surface forced transformations are given by:

$$F_\Theta^{\text{sfc}}(\Theta^*, S, t) = \int \Pi(\Theta, \Theta^*) \Pi(S, S^*) \frac{Q_{\text{net}}}{\rho C_p} \, dA, \quad (6)$$

$$F_S^{\text{sfc}}(\Theta, S^*, t) = \int \Pi(\Theta, \Theta^*) \Pi(S, S^*) f_{\text{net}} \, dA, \quad (7)$$

where Q_{net} is the net surface heat flux, f_{net} is the net surface freshwater flux (including evaporation, precipitation, sea ice

melting/freezing and river runoff), ρ is seawater density at the surface, and C_p is the specific heat capacity of seawater. In the ORCA0083-N06 hindcast, surface salinity restoring is applied, and its contribution is therefore implicitly included in the diagnosed net surface freshwater flux.

The volume $V_{S\Theta}$ can be calculated from the temperature and salinity fields within the Arctic Ocean domain, while the net advective transport $M_{S\Theta}$ is calculated using velocity, temperature, and salinity across the four major Arctic gateways. We use a bin spacing of $\Delta\sigma_0 = 0.025 \text{ kg m}^{-3}$ and following Evans et al. (2014), we use a resolution in T - S space such that the contribution of changes in T and S are approximately similar in density space: $\Delta\Theta = 0.1 \text{ }^\circ\text{C}$ and $\Delta S = 0.01 \text{ g kg}^{-1}$. From the volume change and boundary fluxes, the water mass transformation divergence G_Θ , G_S is calculated using the inverse methods introduced in Evans et al. (2014). The surface forced transformations F_Θ^{sfc} and F_S^{sfc} are then computed using net surface heat flux and freshwater flux, respectively. F_Θ^{res} and F_S^{res} are computed as residuals after calculating all other terms in Eq. (3). These residuals are commonly interpreted as the contributions from interior mixing along temperature and salinity coordinates, though they may also include other unresolved processes such as changes due to penetrative shortwave radiation, as well as transformations from cabbeling and thermobaricity resulting from the nonlinearity of the equation of state (Groeskamp et al., 2019; Nurser and Griffies, 2019; Buckley et al., 2023; Evans et al., 2023; Zou et al., 2024).

2.3 Lagrangian tracking

To analyze the pathways, timescales, and locations of water mass transformation of the Arctic overturning circulation in the ORCA0083-N06 hindcast, we trace waters entering the Arctic Ocean through the four gateways using TRACMASS version 7.0 (Döös et al., 2017; Aldama-Campino et al., 2020). TRACMASS solves the trajectories of parcels through each model grid cell analytically by assuming that the velocity field varies linearly in time (between output time steps) and space (between opposite grid cell walls). An important property of the algorithm is that it conserves mass, or in the case of NEMO, volume, such that each trajectory retains a constant volume transport throughout the tracking. This makes it possible to calculate Lagrangian streamfunctions, and thereby decompose the total Eulerian Arctic overturning streamfunction into contributions from different pathways (Berglund et al., 2023; Tooth et al., 2024). We do not add any stochastic diffusion to the trajectories as this would break volume conservation, and instead follow the resolved advective pathways in the model.

For the Lagrangian tracing experiment, we calculate the average annual cycle over 1979–2015. We start trajectories at all grid cells across the four Arctic gateways every month. To obtain a sufficient resolution, we assign each trajectory a maximum volume transport of $2500 \text{ m}^3 \text{ s}^{-1}$. If the vol-

ume transport in a model grid cell exceeds this value, multiple trajectories are started in that grid cell. In total, around 150 000 trajectories are started. We track the trajectories forward in time using the climatological monthly velocity and tracer fields. We chose to use climatology as input to represent an average picture of the Arctic overturning circulation. We have tested using monthly and 5-daily time-evolving input and looping the period 1979–2015 instead, and the main results did not qualitatively change (not shown). Trajectories are terminated either if they exit the Arctic by returning to the inflow gateways, or after 500 years. We calculate Lagrangian streamfunctions following Tooth et al. (2024). To quantify water mass transformation along the pathways, we calculate the Lagrangian mass, heat and salt divergence for each grid box, following Berglund et al. (2017) and Dey et al. (2024).

3 Results

3.1 Overturning in density-space

We will first quantify the time-mean water mass transformation for the Arctic Ocean, with a particular focus on the overturning circulation. We start by considering the overturning streamfunction in density (σ) space (Fig. 2a), obtained by integrating $M(\sigma^*)$ over σ . The overturning streamfunction has a local minimum and a local maximum, indicating the presence of both a negative and a positive overturning cell, which are referred to as the estuarine and thermal overturning cells, respectively (Haine, 2021). The estuarine cell has a minimum of -0.96 Sv at $\sigma_0 = 27.0 \text{ kg m}^{-3}$, while the thermal cell reaches a maximum of 3.09 Sv at $\sigma_0 = 27.95 \text{ kg m}^{-3}$. The Arctic Ocean thus densifies inflowing waters at a rate approximately three times greater than it lightens them. Compared to the observation-based estimate of Tsubouchi et al. (2024), the thermal cell is slightly stronger but agrees well in density structure, whereas the estuarine cell is weaker and peaks at a lower density, as well as extending through a much lower density level of approximately $\sigma_0 = 25.0 \text{ kg m}^{-3}$. Finally, Tsubouchi et al. (2024) find a third cell, which represents the transformation of Pacific Waters to a denser outflow. This third cell is likely obscured in the hindcast by the large amounts of export of waters between $\sigma_0 = 25.0 \text{ kg m}^{-3}$ and $\sigma_0 = 26.5 \text{ kg m}^{-3}$. Overall, however, there is good agreement between ORCA0083-N06 and that inferred from available observations.

The volume tendency $\frac{dV_\sigma}{dt}$ in the Arctic Ocean is generally small, except for $\sigma_0 > 27.75\text{--}28.0 \text{ kg m}^{-3}$, where there is net water mass formation (Fig. 2b), and $\sigma_0 > 28.0\text{--}28.1 \text{ kg m}^{-3}$, where there is net water mass destruction. This hints at a long term trend of buoyancy gain in the Arctic Ocean deep waters. The source of this buoyancy gain is not investigated here, but we note that it is consistent with an observed warming of deep waters in Fram Strait (Karam et al., 2024). The diapycnal transformation due to surface buoyancy

fluxes, F_σ^{sfc} , is directed toward higher densities across nearly all density classes and reaches a maximum of -2.32 Sv at $\sigma_0 = 27.75 \text{ kg m}^{-3}$ (Fig. 2a), peaking at a lower density than the overturning. Surface forcing contributes to the destruction of water masses lighter than $\sigma_0 < 27.75 \text{ kg m}^{-3}$, and to the production of water masses in the range $\sigma_0 = 27.75\text{--}28.1 \text{ kg m}^{-3}$. Notably, it contributes substantially to the formation of dense waters around $\sigma_0 = 28.0 \text{ kg m}^{-3}$, which are exported from the Arctic as part of the dense outflow, suggesting that surface buoyancy forcing is most important for the thermal cell. We find that cooling as a result of both air-sea heat loss and ice melt dominates the surface-forced densification signal (Fig. A2). The heat-flux component drives densification at a rate of approximately -3.7 Sv at the peak of F_σ^{sfc} . This is nearly three times larger in magnitude than the freshwater contribution, which acts to lighten dense waters at a rate of approximately 1.4 Sv .

The residual transformation F_σ^{res} (interpreted as mixing) shows a more complex structure (Fig. 2b). At lower densities, specifically below $\sigma_0 = 27.7 \text{ kg m}^{-3}$, mixing drives water mass formation with the characteristics of lighter surface polar waters, supplying the majority of the waters exported as part of the estuarine circulation cell. Mixing then acts destructively over a broad intermediate density range, with pronounced water mass destruction between $\sigma_0 = 27.7\text{--}27.95 \text{ kg m}^{-3}$ (Fig. 2b), corresponding to a part of the Atlantic Water inflow. The lighter fraction of this destruction contributes to the estuarine cell by mixing Atlantic Water upward into fresher surface layers, while the denser fraction, along with the destruction observed at the upper end of the density range for $\sigma_0 > 28.05 \text{ kg m}^{-3}$, leads to a net convergence of transformation around $\sigma_0 = 28.0\text{--}28.05 \text{ kg m}^{-3}$. This convergence corresponds to the majority of dense water mass exports, suggesting that while surface fluxes can provide much of the required densification to sustain the Arctic overturning circulation, preconditioning the inflowing waters, mixing sets the final properties of the dense waters that are exported from the Arctic Ocean through its deeper branches, analogous to the findings of Evans et al. (2023) for the formation of North Atlantic Deep Water.

3.2 Overturning in temperature–salinity space

While the water mass transformation in density space offers general insights into the transformations required to sustain the Arctic overturning circulation, a diagnosis of the water mass transformation in temperature–salinity ($T\text{--}S$) space permits a more detailed, process based analysis (Pemberton et al., 2015; Hieronymus et al., 2014). The time-mean volume distribution of the Arctic Ocean $T\text{--}S$ as well as some of the key water masses are visualized in Fig. 3. In this section, as before, we place a special focus on the thermal branch of the Arctic overturning circulation and the water mass transformation processes that support it. We will start by considering the time-mean overturning divergence $M_{S\Theta}$ (Fig. 4, col-

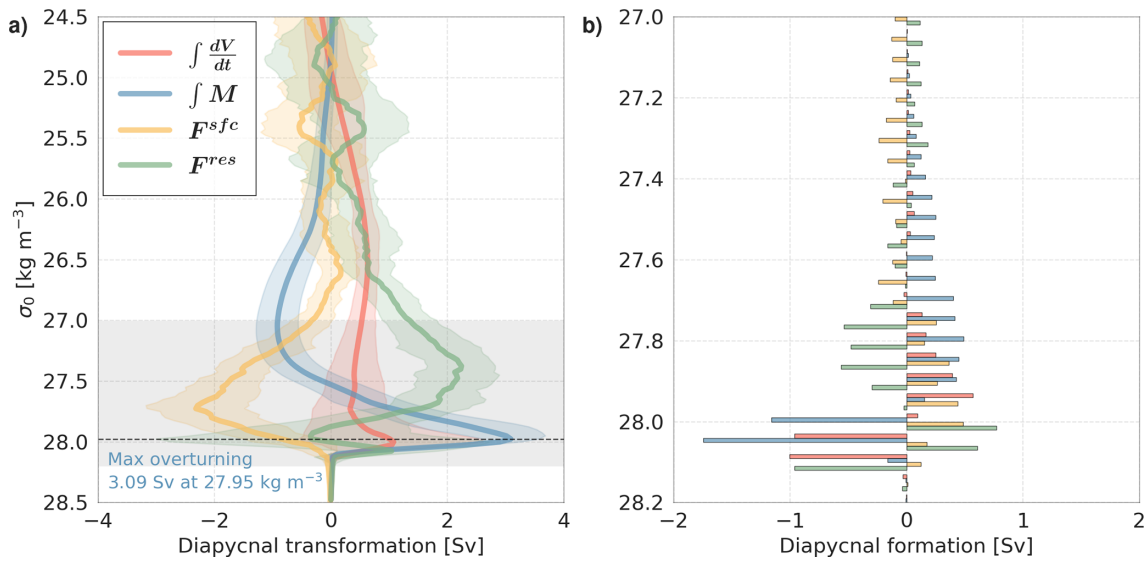


Figure 2. Time-mean diapycnal water mass transformation (a) and formation (b) for the Arctic Ocean from 1979–2015. The respective colors represent the integrated volume tendency (red), the overturning streamfunction (blue), the surface forced transformation (yellow) and the residual transformation (green), as well as their yearly standard deviation in shading. The quantities in (b) are calculated as the divergence of those in (a). The gray shading in (a) represents the extent of the y axis in (b).

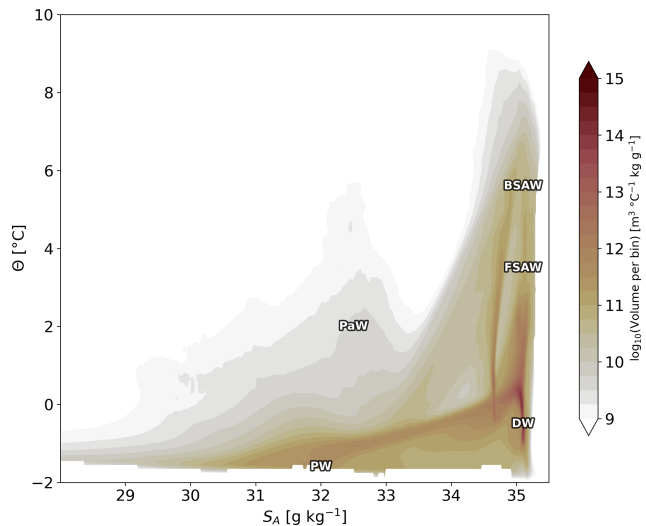


Figure 3. Time-mean volumetric T – S distribution in the Arctic Ocean. The major water masses are marked by their abbreviations: Barents Sea Atlantic Water (BSAW), Fram Strait Atlantic Water (FSAW), Pacific Water (PaW), Dense Water (DW) and Polar Water (PW).

ors) and the water mass transformation $G_{S\Theta}$ (Fig. 4, vectors) required to support it. The use of thermohaline coordinates reveals the presence of the Pacific cell (Tsubouchi et al., 2024), where relatively warm and fresh Bering Strait inflow ($\Theta = -2\text{--}7\text{ }^{\circ}\text{C}$ and $S = 32\text{--}33\text{ g kg}^{-1}$), undergoes a predominantly cooling transformation shown by the vectors in Fig. 4. This cell's presence is obscured in σ -space (Fig. 2).

We first turn our focus to the estuarine circulation cell, which governs the net freshwater export from the Arctic Ocean (Rudels and Carmack, 2022). In contrast to the comparatively small Pacific cell, the estuarine cell exhibits a more persistent structure in both σ space and T – S space. In T – S space, however, it is characterized by two distinct branches (visible as two blue curves converging on the freezing line in Fig. 4), corresponding to different Arctic outflow pathways. Both branches export Polar Waters, defined here by near-freezing temperatures and relatively low salinities ($S = 31\text{--}34\text{ g kg}^{-1}$). While their exported properties are broadly similar, the branches differ in their source waters and transformation pathways.

The warmer branch originates primarily from Atlantic Water inflows ($S > 34.5\text{ g kg}^{-1}$, $\Theta > 5\text{ }^{\circ}\text{C}$) entering through the Barents Sea Opening and Davis Strait (not shown). In T – S space, the pathway of this branch reflects progressive modification of warm, saline Atlantic inflows through cooling and dilution by fresher surface waters, sea-ice melt, and runoff. This results in outflowing Polar Waters of approximately $S \approx 31\text{--}33\text{ g kg}^{-1}$. The colder branch is fed predominantly by denser and cooler Atlantic Waters ($S > 35\text{ g kg}^{-1}$, $\Theta > 0\text{ }^{\circ}\text{C}$). These waters undergo substantial modification through mixing with fresher local waters as well as freshwater inputs from ice melt, producing an outflow that likewise emerges as Polar Water but with slightly higher maximum salinities ($S \approx 34\text{ g kg}^{-1}$).

Next, we consider the thermal overturning cell, which occupies a relatively narrow density range ($\sigma = 27.5\text{--}28.2$), yet dominates the Arctic's volume transport. This cell is primarily driven by the inflow of warm, saline Atlantic waters

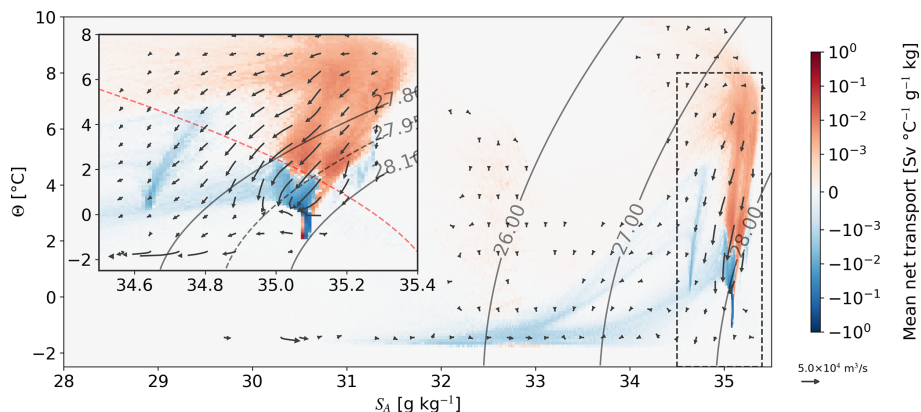


Figure 4. Time-mean diathermohaline net advective transport $M_{S\Theta}$ (colors) and water mass transformation $G_{S\Theta}$ (vectors) for the Arctic Ocean from 1979–2015. The colors represent net inflow (red) and net outflow (blue) per $T-S$ bin. The arrows represent the combined transformation in both diathermal (vertical) and dihaline (horizontal) directions. The inset focuses on the thermal overturning cell's $T-S$ ranges. The dashed contours represent the density (black) and spiciness (red) of maximum overturning strength.

($\Theta > 2^\circ\text{C}$ and $S > 35 \text{ g kg}^{-1}$), which separate into two distinct branches in $T-S$ space: the denser, cooler, and slightly fresher Fram Strait Branch ($\Theta = 2\text{--}5^\circ\text{C}$) and the lighter, warmer ($\Theta > 4^\circ\text{C}$), and saltier Barents Sea Branch. The water mass transformation, $G_{S\Theta}$, highlights the transformation from inflow to outflow properties (Fig. 4, vectors). While both branches undergo net cooling with slight freshening, the warmer waters entering as part of the Barents Sea Branch experience the most substantial transformation, ultimately converging toward the cold, dense Fram Strait outflow ($-1 < \Theta < 1^\circ\text{C}$, $35.0 < S < 35.1 \text{ g kg}^{-1}$). This outflow forms the primary deep limb of the Arctic overturning circulation.

As the thermal cell dominates volume transports and concerns mainly inflowing Atlantic Water and densified outflows of similar salinity, it is instructive for a process-based analysis to limit our focus to the specific transformation processes in the range of T and S values corresponding to the thermal overturning cell. To that end, we consider the components of the decomposed WMT: the surface forced WMT $F_{S\Theta}^{\text{sfc}}$ and the residual WMT $F_{S\Theta}^{\text{res}}$ (Eq. 5, Fig. 5). The decomposition reveals that in the time-mean, the Atlantic Water inflowing as part of the Barents Sea Branch ($S > 35 \text{ g kg}^{-1}$, $\Theta > 4^\circ\text{C}$), undergoes substantial cooling due to air-sea heat fluxes. Surface cooling is the dominant process until they reach approximately 2.5°C , below which ice melt becomes increasingly important, indicated by the transformation vectors bending towards lower salinities due to the addition of freshwater (Fig. 5a). This transformation results in the highly effective destruction of large volumes of warm inflow waters, consistent with a large surface forced diapycnal transformation in Fig. 2. As such, the Barents Sea expectedly dominates the surface forced component. Conversely, the Fram Strait Branch is cooled to a lesser extent, though both branches ultimately contribute to the formation of substantial volumes of dense waters ($\sigma > 27.75 \text{ kg m}^{-3}$) spanning a broad range

of $T-S$ characteristics. We further see both strong formation and destruction of waters near the freezing point, which is related to the seasonal melting and freezing cycle. Finally, surface forcing is responsible for the production of the densest waters found in the Arctic: the highly saline, near freezing point Barents Sea dense waters ($S > 35.1 \text{ g kg}^{-1}$, $\sigma > 28.1 \text{ kg m}^{-3}$) (Årthun et al., 2011).

The residual component, on the other hand, is much more clearly associated with a net freshening of the inflowing salty Atlantic Water (Fig. 5b). Here we interpret the residual component as the contribution from ocean mixing, but make no explicit distinction between vertical mixing or horizontal mixing. However, the orientation of the thermohaline transformation vectors with respect to the isopycnals drawn in Fig. 5b leaves clues as to the nature of the relevant mixing processes. Transformation vectors aligned parallel to isopycnals imply purely isopycnal mixing, while those oriented perpendicular to isopycnals are indicative of diapycnal mixing.

Firstly, mixing leads to a seasonal transformation near the freezing point that opposes the effect of surface forcing. These opposing effects largely cancel, resulting in little net impact of much of the melting and freezing cycle on the Arctic WMT. Meanwhile, both inflow branches experience freshening, but there is more destruction of waters that have properties associated with the Fram Strait Branch. Notably, there is substantial net destruction of waters with temperature characteristics ($\Theta = 1.5\text{--}3^\circ\text{C}$) corresponding to Fram Strait inflow waters. While these waters undergo both isopycnal and diapycnal modification, the distinct isopycnal component suggests that isopycnal mixing plays an important role in modulating the Fram Strait Branch properties. Parts of the inflowing Fram Strait Branch waters are only slightly modified (cooled and freshened) to produce the mixing convergence at $S > 35 \text{ g kg}^{-1}$, $\Theta = 1.5\text{--}2^\circ\text{C}$, which cor-

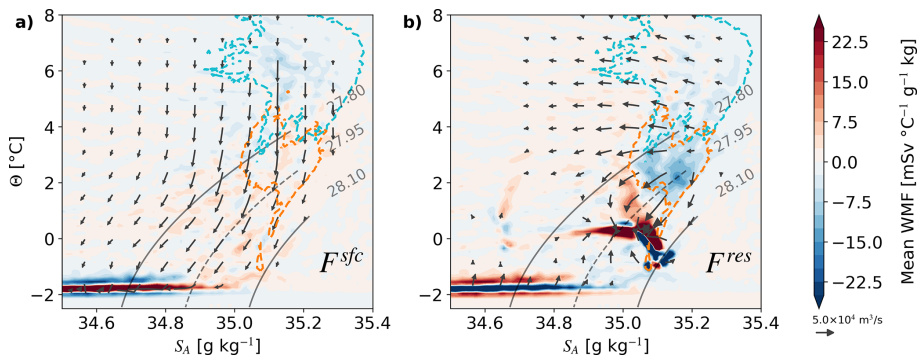


Figure 5. Time-mean surface forced (a) and residual components (b) of the diathermalhaline water mass transformation for the Arctic Ocean from 1979–2015. The colors represent water mass formation (red) and water mass destruction (blue). The arrows represent the combined transformation in both diathermal (vertical) and dihaline (horizontal) directions. The dashed contours represent the density of maximum overturning strength (black), as well as the approximate Fram Strait (orange) and Barents Sea (cyan) inflow ($M_{S\Theta} > 2 \text{ mSv } ^\circ\text{C}^{-1} \text{ g}^{-1} \text{ kg}$ at the respective gateways).

responds to the outflow on the same thermohaline properties in Fig. 4. We identify this as recirculating Atlantic Water, flowing westwards relatively quickly after entering the Arctic Ocean. These Atlantic Waters are likely mixed with colder and fresher halocline waters or shelf waters near the shelf break (Saloranta et al., 2004; Ivanov et al., 2024). In agreement with observations (Cottier and Venables, 2007), the curvature of the transformation arrows in T – S space towards higher densities additionally suggests the possibility of cabbeling as a relevant transformation and densification process for the Fram Strait Atlantic Water.

Figure 5 furthermore shows the destruction through mixing of a cold and salty water mass ($S = 34.85\text{--}35.1 \text{ g kg}^{-1}$, $\Theta < -0.5 \text{ }^\circ\text{C}$). A regional decomposition (not shown) shows this water mass is seasonally produced during winter in the Barents Sea (see also Fig. 11). Vectors indicate that these cold and salty Barents Sea waters mix with Atlantic Water originating from Fram Strait. Being denser than the Fram Strait inflow, these waters likely contribute to the additional densification required for the transformation of Atlantic Water to the outflow density. Finally, mixing leads to a general convergence around the dense outflow waters ($\Theta = -1\text{--}0 \text{ }^\circ\text{C}$, $S \approx 35.1 \text{ g kg}^{-1}$) that ultimately exit through Fram Strait. This convergence requires contributions from both diapycnal and isopycnal mixing processes. Thus, surface forcing preconditions the inflowing Atlantic Water, generating large volumes of water near the outflow density, particularly from Barents Sea inflows. However, mixing ultimately sets the final T – S properties of the dense outflow by homogenizing waters from the two inflow branches. Importantly, the relevant mixing processes are largely obscured by considering only the WMT in density space.

3.3 Overturning pathways and time scales

After analyzing the Arctic overturning in density and T – S space, we next analyze the contributions of the different in-

flows at the gateways and the pathways of waters between the gateways. First, we decompose the total Eulerian overturning streamfunction into the net contribution from each of the four gateways (Fig. 6a). Most of the lighter waters ($\sigma_0 < 27 \text{ kg m}^{-3}$) enter the Arctic through Bering Strait and the Barents Sea, and exit the Arctic through Davis Strait and Fram Strait. More lighter waters exit Fram Strait in the hindcast than in the estimates from Tsubouchi et al. (2024). Most of the denser, Atlantic Waters ($27.4 \text{ kg m}^{-3} < \sigma_0 < 27.8 \text{ kg m}^{-3}$) enter the Arctic through the Barents Sea and Fram Strait, and the Dense Waters ($\sigma_0 > 27.95 \text{ kg m}^{-3}$) leave through Fram Strait. The net dense overturning across the Barents Sea Opening and Fram Strait is in good agreement with the estimates from Tsubouchi et al. (2024), showing that the dense overturning and outflow of densified waters is dominated by Fram Strait.

The analysis in T – S space indicated that both the Fram Strait and the Barents Sea branch contribute to the dense overturning across Fram Strait. To more accurately quantify the relative importance of the two branches, and along which pathways the waters are transformed, we use Lagrangian trajectories (Sect. 2.3), and explicitly track waters entering the four gateways. We calculate a Lagrangian streamfunction in a similar way to the Eulerian streamfunction by binning the volume transport as trajectories enter the Arctic (inflow) and as they exit the Arctic (outflow) into density bins ($\Delta\sigma_0 = 0.01 \text{ kg m}^{-3}$), calculating the net transport for each density bin, and integrating over density. The total Lagrangian streamfunction of all trajectories entering the Arctic (Fig. 6b) is very similar to the Eulerian streamfunction (Fig. 6a). Note that the Lagrangian streamfunctions are closed, since the trajectories conserve their volume transport along the way. We then decompose the streamfunction into the different inflow pathways by selecting only the trajectories that start at the different gateways. Dense overturning is dominated by the Barents Sea Branch (e.g. water en-

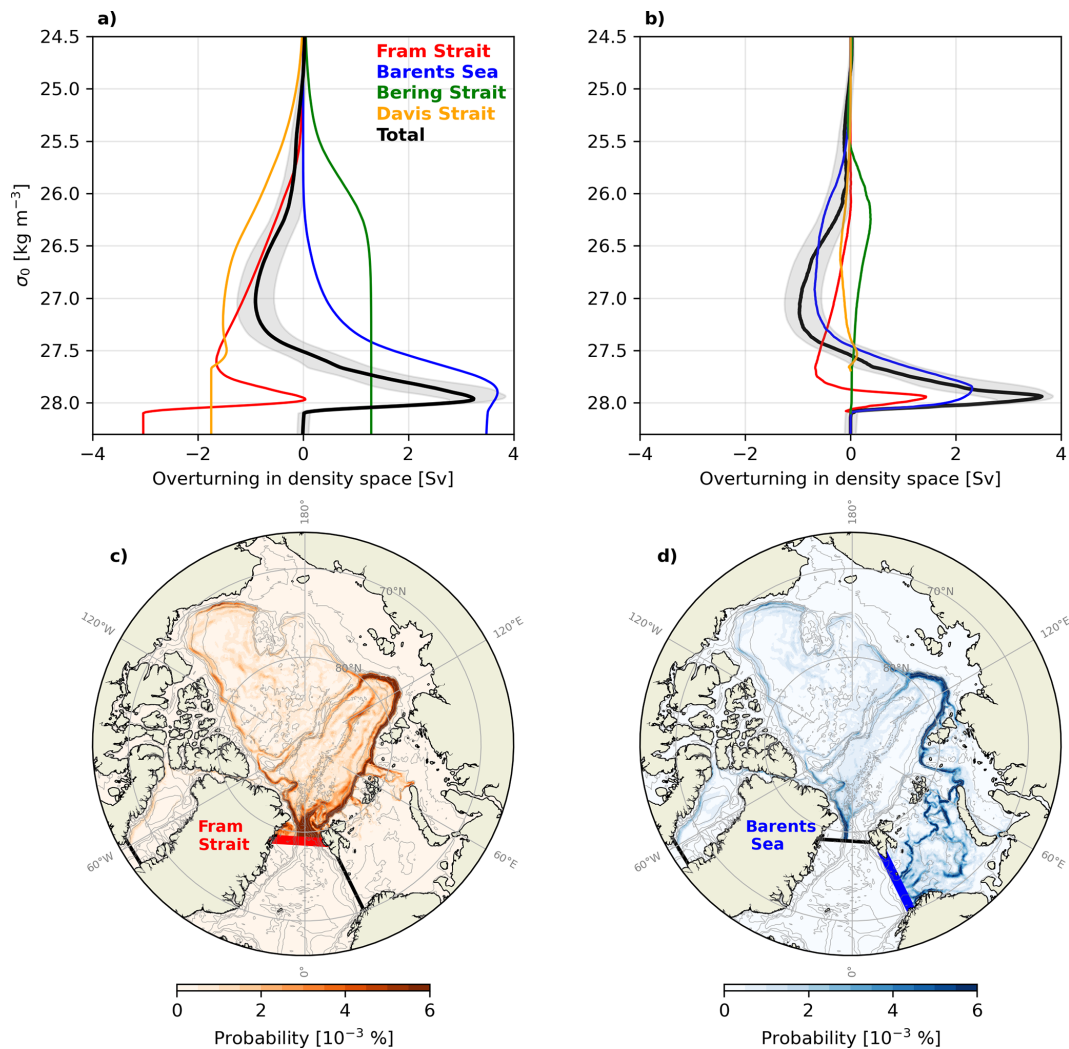


Figure 6. Eulerian and Lagrangian decomposition of Arctic overturning. **(a)** Time mean Eulerian streamfunction across the Arctic gateways in ORCA0083-N06, and split into the net overturning across each gateway. **(b)** Lagrangian overturning streamfunction for trajectories started at each gateway, until exiting the Arctic Ocean. Maps of trajectory probability for trajectories started at **(c)** Fram Strait and **(d)** the Barents Sea Opening.

tering the Barents Sea and exiting Fram Strait), while the Fram Strait Branch has a major contribution at very high densities ($\sigma_0 > 27.8 \text{ kg m}^{-3}$; Fig. 6b). Comparing the values of the streamfunctions at the density of maximum overturning (27.95 kg m^{-3}), approximately 60 % of Dense Water produced in the Arctic Ocean originates from the Barents Sea, and approximately 40 % originates from Fram Strait itself. Furthermore, most of the water in the estuarine cell ($\sigma_0 < 27.5 \text{ kg m}^{-3}$) originates from the Barents Sea and Davis Strait, which has mixed with fresher Arctic origin waters. Fram Strait waters also contribute to the estuarine cell, but at higher densities ($\sigma_0 > 27 \text{ kg m}^{-3}$) and therefore mostly to the colder estuarine branch found in Fig. 4. Finally, the Pacific overturning cell identified by Tsubouchi et al. (2024)

and in Fig. 4 emerges in the Lagrangian decomposition, but is hidden in the total overturning streamfunction.

The pathways of trajectories entering the Arctic at the two Atlantic Water gateways are shown in Fig. 6c and d. Approximately 60 % of the water entering Fram Strait recirculates and quickly flows back south. The rest largely follows the Atlantic Water Boundary Current (AWBC) eastwards along the rim of the Eurasian Basin (as indicated in Fig. 1). Waters originating in the Barents Sea mostly enter the Arctic Ocean at St. Anna trough, where they merge with the AWBC. Further into the Arctic, north of the Laptev Sea, part of the Atlantic Water turns north and follows either the Lomonosov Ridge or the Gakkel Ridge, thereby recirculating in the Eurasian basin, whereas another part continues along the AWBC into the Amerasian Basin. These pathways are

consistent with existing studies of the pathways of Atlantic Water in the Arctic (e.g. Timmermans and Marshall, 2020; Rudels and Carmack, 2022; Pasqualini et al., 2024).

Next, we briefly analyze the time scales of the Arctic overturning circulation. We calculate the Lagrangian streamfunction as before, but now decompose it into different transit times, based on how long the trajectories take to exit the Arctic (Fig. 7). Waters densifying and recirculating north of Fram Strait within less than 10 years contribute approximately 10 % to the total maximum overturning. Waters recirculating in the Eurasian basin and following either the Lomonosov or Gakkel ridge back to Fram Strait take 10–20 years and contribute another 25 % to the total overturning. This time scale is consistent with tracer studies of intermediate Atlantic Water circulation in the Eurasian basin (Wefing et al., 2021; Pasqualini et al., 2024). Approximately 65 % of the total Arctic overturning is made up of water that takes longer than 20 years to exit the Arctic Ocean. In addition to trajectories circulating in the Eurasian basin for several decades, this also includes trajectories entering the Amersasian Basin and circumnavigating the entire deep Arctic basin. This indicates that most Atlantic Water will take multiple decades to exit Fram Strait as Dense Water and contribute to the lower limb of the AMOC.

The Arctic estuarine cell ($\sigma_0 = 27.0 \text{ kg m}^{-3}$) has much shorter time scales, and most of the lighter waters exit the Arctic after 10–20 years. Here, the shortest pathway is the transpolar drift, a surface circulation feature that connects the Siberian Arctic to Fram Strait (not shown).

3.4 Geographical location of water mass transformation

The results in Sect. 3.1 show that the transformation of Atlantic Waters into Dense Waters is dominated by surface cooling (Fig. 2). Mixing is driving the transformation into lighter polar waters and also plays a role in producing very dense overflow waters. Here, we remap the diapycnal water mass transformation from density space into geographical space to understand the importance of the two main pathways of Atlantic Water in the Arctic. First, we remap the surface-forced water mass transformation into geographical space. Second, we calculate where transformation occurs along the pathways of the water entering the Arctic Ocean via Fram Strait and the Barents Sea, using the Lagrangian trajectories. Third, to distinguish between the surface forced and the internal mixing component, we compare this total (Lagrangian) transformation with the (Eulerian) surface transformation, thereby combining the Lagrangian and Eulerian approaches.

We start with the surface forced water mass transformation (Fig. 8). The strongest transformation occurs in the Barents Sea and northwest of Svalbard, along the main inflow pathways of the Atlantic Water through Fram Strait and the Barents Sea Opening (Athanase et al., 2020; Skagseth

et al., 2020). Most of the transformation in these areas occurs through surface cooling and through interaction with sea-ice melt and freeze. Negative surface transformation through sea-ice melt is largest north of Fram Strait. Further into the Arctic, the surface forcing is small, as those areas are permanently sea-ice covered and the warm Atlantic Waters are sheltered from the surface by the cold halocline (Aagaard et al., 1981).

Next, we look at the total water mass transformation in the Lagrangian experiment. For a given grid cell, we sum up the density change for all trajectories that pass through that grid cell, obtaining spatial maps of density divergence, or mass flux (Fig. 9). For water entering via Fram Strait, a large part of the water mass transformation occurs close to Fram Strait (Fig. 9a). Waters flowing into the Arctic immediately northwest of Svalbard gain density due to surface cooling (Fig. 8), as these pathways are partly ice-free in winter (Athanase et al., 2020). Waters leaving the Arctic on the western side of Fram Strait also gain density on their way, while waters flowing north along the shelf break around the Yermak Plateau lose density. Because northwestern Fram Strait is usually ice-covered, this density change is likely through sea-ice melt (Fig. 8) and interaction between the inflowing Atlantic Waters and the outflowing Polar Waters or modified and recirculating Atlantic Waters. Mixing of these water masses cools and freshens the inflowing Atlantic Waters, and warms and salinifies the outflowing waters (Figs. A3 and A4). Overall, the salinity change dominates the density changes, such that Atlantic Water is becoming lighter and the outflowing waters become denser.

Further downstream, the Fram Strait branch waters slowly become less dense as they transit through the Arctic. Notable exceptions are found along the AWBC in the Nansen Basin, where waters gain density north of Franz Joseph Land and east of St. Anna trough. Those locations coincide with troughs in the shelf break in the northern Barents and Kara seas, where the Fram Strait branch interacts with waters originating in the Barents Sea (Schauer et al., 2002; Ivanov et al., 2024), and where the mass divergence shows a density loss for Barents branch waters (Fig. 9b). This indicates that the interaction between the two Atlantic Water branches transforms some of the Fram Strait branch waters into denser waters, and contributes to the dense water formation along the Fram Strait pathway, consistent with results in Sect. 3.2. Analysis of the heat and salinity change shows that the heat exchange between the two branches dominates the density signal in these regions (Figs. 5b, A3, and A4).

Waters entering the Barents Sea undergo a strong density increase in the Barents Sea as they are cooled (Fig. 9b), consistent with Fig. 8. Beyond the Barents Sea, waters decrease their density along the Siberian shelves, most strongly close to the outflows of Siberian rivers, where they mix with the fresh riverine water, decreasing their salinity (Fig. A4). Water that becomes lighter will mostly follow the transpolar drift and eventually exit the Arctic with a lower density, contribut-

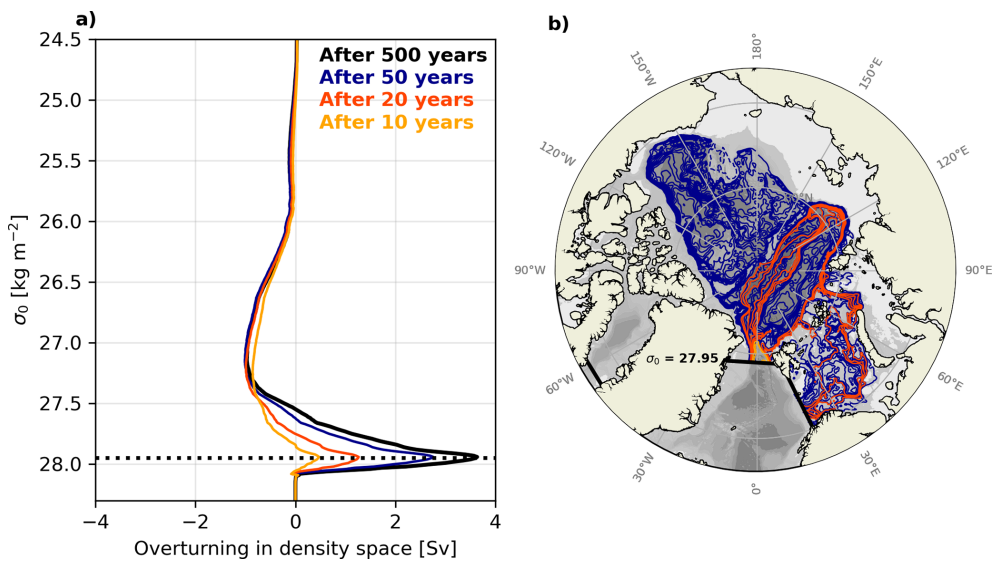


Figure 7. Timescales of the Arctic overturning circulation. **(a)** Lagrangian Arctic overturning streamfunction for all trajectories leaving the Arctic after 10, 20, and 50 years, and over the entire 500 years of the Lagrangian experiment in ORCA0083-N06. **(b)** Map showing the barotropic streamfunctions Ψ of trajectories overturning at 27.95 kg m^{-3} (i.e. enter the Arctic Ocean below this density and leave it above this density; dashed line in **(a)**). The different colors correspond to the time scales in **(a)**. Ψ is set to zero over Greenland and the contour interval is 0.1 Sv .

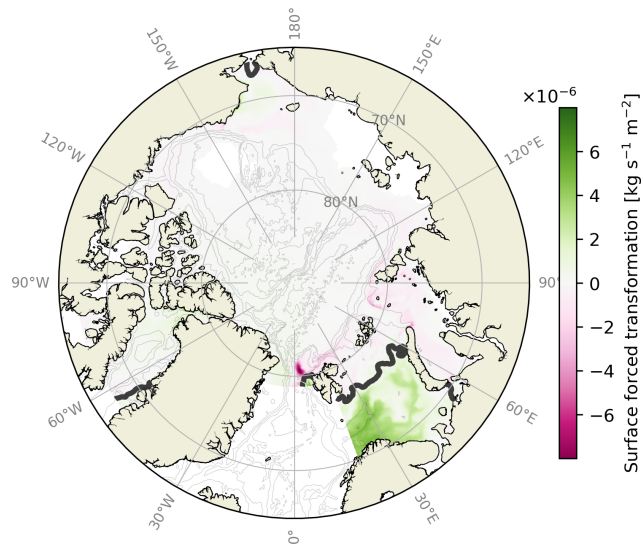


Figure 8. Locations of surface water mass transformation. Total surface-forced water mass transformation integrated over all density classes and averaged over 1979–2015 in ORCA0083-N06. The thick black line indicates the time-averaged sea ice cover (where there is more than 50 % sea ice presence).

ing to the estuarine cell. Before exiting the Arctic, just north of Fram Strait, those waters increase their density again, most likely by mixing with the inflowing and recirculating Atlantic Waters in the central Fram Strait, which, as shown above, experience a decrease in density (Fig. 9a).

Lastly, waters from both branches decrease their density in the boundary current north of Alaska (Fig. 9a and b). Here, they mostly interact with fresher Pacific Waters originating from Bering Strait that enter the Amerasian Basin from the Chukchi Shelf, or that circulate in the Beaufort Gyre, and ventilate the Arctic halocline (Aagaard et al., 1981).

Next, we focus on the water mass transformation that contributes to the dense overturning circulation by only selecting trajectories that contribute to net overturning at $\sigma_0 = 27.95 \text{ kg m}^{-3}$ (the density of maximum overturning; Fig. 9c and d). Apart from the Barents Sea and the areas north of Svalbard, most locations of transformation for both branches are now over the Atlantic Water Boundary Current (AWBC). Waters originating from Fram Strait increase their density along most of their path along the AWBC, and notably north of Franz Joseph Land and St. Anna trough, where they, as discussed, likely interact with Barents Sea waters. Waters originating from the Barents Sea increase in density within the Barents Sea, and decrease in density downstream where they interact with the Fram Strait branch.

Further downstream in the Laptev Sea, Barents Sea origin waters in the boundary current increase their density (Fig. 9d). The Laptev shelf is a known area of high sea-ice production and formation of dense shelf waters (Cornish et al., 2022), which could mix with the Atlantic Waters in the AWBC and increase their density. An analysis of dense water production over the Laptev shelf in ORCA0083-N06 confirms that there are dense waters produced, although slightly lighter than the density of maximum Arctic overturning (not shown). Another source for the density increase in this re-

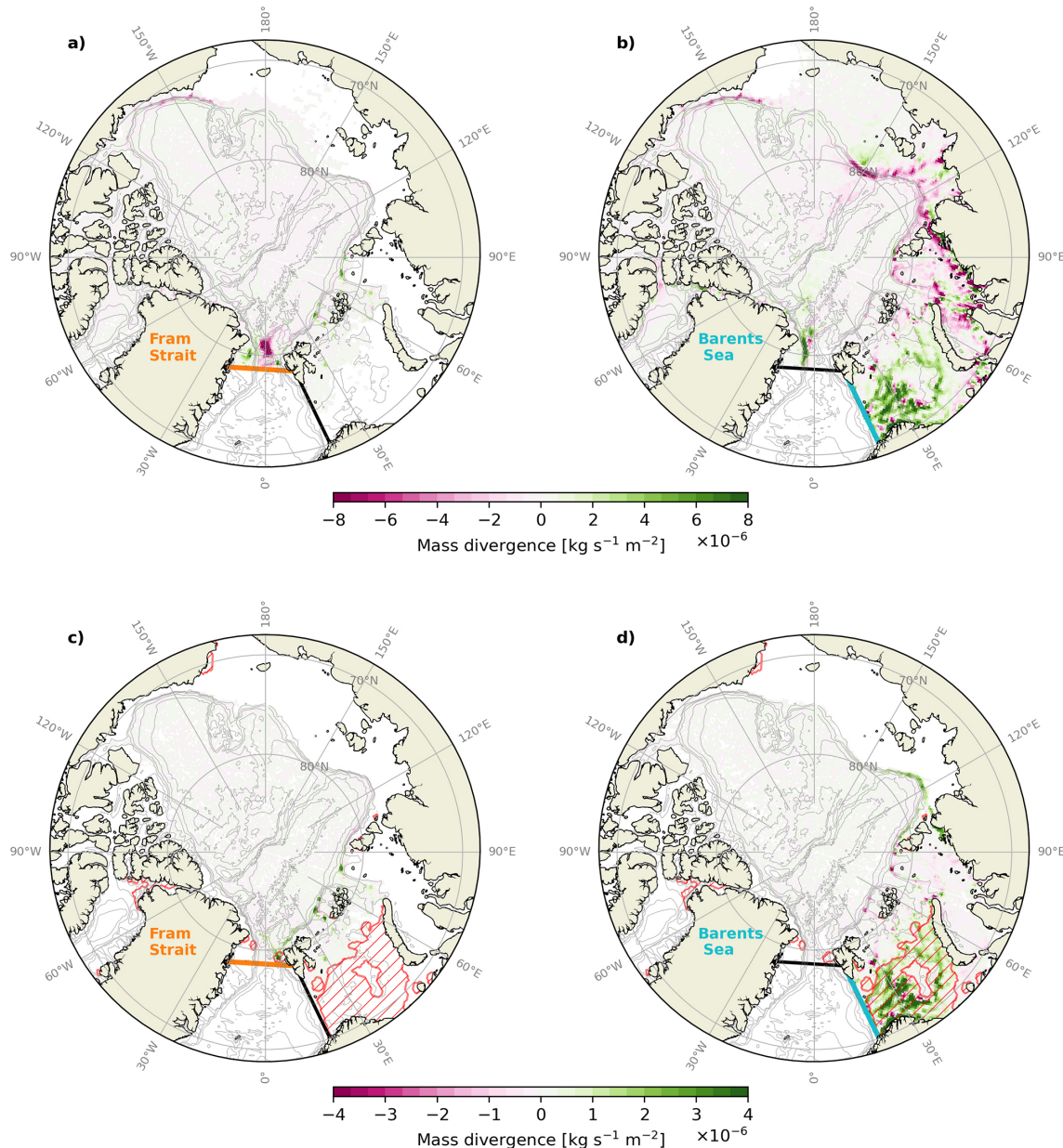


Figure 9. Locations of water mass transformation. Total mass divergence of (a, b) all trajectories entering the Arctic through Fram Strait and the Barents Sea and (c, d) for trajectories overturning at 27.95 kg m^{-3} (i.e. entering the Arctic below this density, and leaving it above this density). Values are normalized by the grid cell area. Green colors indicate mass (density) gain, purple colors indicate mass loss. Hatched red area indicate regions where surface-forced transformation in Fig. 8 is larger than $1 \times 10^{-6} \text{ kg s}^{-1} \text{ m}^{-2}$, which are used to calculate the contribution of surface forcing to water mass transformation.

gion is Barents and Kara Sea origin waters that flow through Vilkitsky Strait, gain density on the shelf, and then mix with the waters in the AWBC (Fig. 9d; Janout et al., 2017).

As a last step, we combine the surface forced transformation in Fig. 8 and the total Lagrangian transformation in Fig. 9c and d to produce a rough estimate of the relative contributions of surface forcing and internal mixing in driving water mass transformation at the density of maximum overturning. We do so by determining the regions with sub-

stantial surface forcing (more than $+1 \times 10^{-6} \text{ kg s}^{-1} \text{ m}^{-2}$; Fig. 8). The areas meeting this criterion, e.g. the Barents Sea and the region northwest of Svalbard, are indicated in Fig. 9c and d (hatched areas). Assuming that water in those regions will predominantly transform through surface forcing, we sum the transformation from Fig. 9c and d inside the regions and compare them to the transformation outside the regions, which we then assume to be due to internal mixing. Based on this calculation, we estimate that for the dense

overturning cell, approximately 15 % of total transformation for the Fram Strait branch is surface-forced, and approximately 85 % driven by internal mixing. For the Barents Sea branch, approximately 85 % of the transformation is surface-driven, and only approximately 15 % is through internal mixing. These rough estimates are robust to the exact choice of threshold used to define regions of surface forcing. Taking the two branches together gives an estimated total contribution of approximately 25 % from internal mixing to the dense overturning. We emphasize that this is only a rough estimate of the relative role of mixing, and that the exact value will most likely vary over time. However, our rough estimate is consistent with the earlier result that surface forcing dominates the transformation, but internal mixing plays a role at high densities (Figs. 2 and 5).

4 Discussion and Conclusions

The Arctic is the northernmost terminus of the AMOC, and produces some of the densest waters that enter the lower branch of the AMOC (Zhang and Thomas, 2021). Despite its importance, the Arctic overturning circulation remains little explored. Although it is well established that the Arctic Ocean transforms the inflowing warm, salty Atlantic Water into both cold, dense waters, and cold, fresh surface waters (Eldevik and Nilsen, 2013; Pemberton et al., 2015; Rudels et al., 2015; Haine, 2021; Brown et al., 2025), how much transformation occurs and where and by which mechanisms this takes place is still not established. Here, we have quantified the mean structure of the Arctic overturning circulation in the eddy-rich ORCA0083-N06 ocean hindcast between 1979–2015 using an Eulerian water mass transformation framework and Lagrangian experiments. Key results on the transformation mechanisms and locations are summarized in Fig. 10.

We find that Atlantic Water is transformed into dense waters at a rate of 3.1 Sv and into Polar Water at a rate of 1 Sv. Consistent with Pemberton et al. (2015), surface processes mainly act to transform Arctic waters toward colder temperatures, whereas mixing primarily transforms waters toward lower salinities (Fig. 5). The dense overturning is dominated by the Barents Sea branch, which transforms Atlantic Water over a wide range of densities into dense waters, while the Fram Strait branch contributes strongly only to a narrow density range around the density of maximum overturning ($\sigma_0 = 27.95 \text{ kg m}^{-3}$). The dominance of the Barents Sea in the dense water production in the Arctic Ocean confirms earlier work (Smedsrød et al., 2013; Moat et al., 2014). Atlantic Water is transformed into dense waters mostly by surface cooling in the Barents Sea and north of Svalbard (Figs. 5a, 8, and 9). Additionally, interior mixing plays an important role in transforming Atlantic Water into dense waters through two main mechanisms: First, by mixing cold, dense Barents branch waters with warmer and more saline Fram Strait wa-

ters on the shelf break in the Nansen Basin, and in St. Anna Trough at the Barents Sea exit (Figs. 5b and 9c and d). Secondly, Atlantic Waters increase in density by mixing with dense shelf waters in the Kara and Laptev seas. We estimate the contribution of interior mixing to dense overturning to be approximately 25 % in total, with a much higher contribution to the Fram Strait branch and a small contribution to the Barents Sea branch. In contrast, mixing dominates the estuarine branch by mixing Atlantic Waters with fresher waters. This mixing mostly occurs immediately north of Fram Strait, and along the Siberian coast, where the largest rivers enter the Arctic Ocean.

Our finding that interior mixing plays an important role for the estuarine branch, but a smaller role for the dense overturning, is broadly consistent with other model- and observation-based estimates (Bacon et al., 2022; Brown et al., 2025). There are, however, some differences between our results and the observation-based estimates by Brown et al. (2025). Based on observational data combined with an inverse model, Brown et al. (2025) estimate that Atlantic Water is transformed into dense water at a rate of 1.8 Sv. This is substantially weaker than our estimate (3.1 Sv), which agrees more with the observation-based estimate of 2.9 Sv by Tsubouchi et al. (2024) and with estimates by other ocean reanalysis products (Årthun et al., 2025). Although our estimate of Atlantic Water to dense water transformation, and Arctic overturning in general, agree with Tsubouchi et al. (2024), our results highlight the Barents Sea as the main conduit of Atlantic Water (Fig. 6a) whereas Tsubouchi et al. (2024) find Fram Strait to be the most important gateway (their Fig. 4). We note though that the net transports through the Barents Sea Opening and Fram Strait simulated by the model used here are consistent with observations within their uncertainty (Table 1).

While the estimates of Tsubouchi et al. (2024) and Brown et al. (2025) have the advantage of being based on observational data, they also strongly rely on inverse models that require extensive spatial and temporal interpolation of the irregular observations to produce a closed volume budget of the Arctic Ocean and associated streamfunctions. On the other hand, our results are based on a single eddy-rich ocean hindcast. The hindcast is able to realistically simulate key components of the Arctic Ocean circulation (Kelly et al., 2018, 2019), including the Atlantic Water inflows and the pathways, timescales and strength of dense overturning, but has biases related to the Atlantic Water layer temperature and fresh outflows at the gateways (Table 1 and Figs. 6 and A1). One potential source of these biases is that the model does not include tides and is not eddy-resolving on the shelves. The model might thus underestimate mixing (Rippeith et al., 2015; Fer et al., 2015; Janout and Lenn, 2014; Renner et al., 2018). Additionally, the hindcast includes a sea-surface salinity restoring term, which adds an artificial source or sink to the surface freshwater budget. In a similar but lower-resolution model simulation, Pemberton et al.

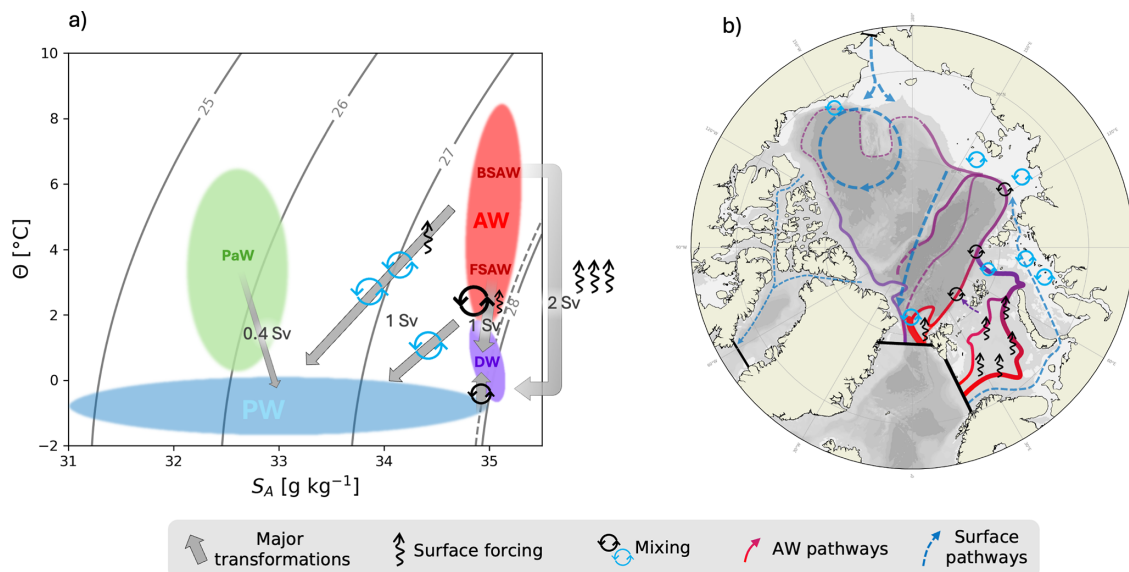


Figure 10. Schematic of the pathways and mechanisms associated with the Arctic overturning circulation. (a) Temperature-salinity diagram showing the major transformations of Atlantic Water (AW) into dense waters (DW) and Polar Waters (PW) and Pacific Water (PaW) into PW. The AW is further split into the Barents Sea (BSAW) and the Fram Strait (FSAW) components. Numbers in Sv indicate the approximate rate of transformations. (b) Map indicating the pathways and locations of transformation, showing that AW is modified by surface forcing (heat loss and ice melt/freeze) in the Barents Sea and north of Svalbard, and further modified by interior mixing mainly with denser water along the boundary current in the Nansen Basin (black circular arrows) and with lighter waters along on the Siberian shelves and north of Fram Strait (blue circular arrows).

(2015) separated the impact of salinity restoring on Arctic water mass transformation, and found the largest impact in a salinity range of 30–32 g kg⁻¹, indicating an influence on the estuarine cell, i.e. the transformation of Atlantic Water into Polar Water. The dense overturning branch, which is the main focus of this study, is less impacted by the surface salinity restoring.

An analysis of the time scales involved in the Arctic overturning circulation shows that most of the dense waters produced along the Fram and Barents Sea branches take multiple decades to exit Fram Strait. This opens the question of how quickly changes in water mass transformation will translate into changes in the overturning strength. Recently, Årthun et al. (2025) found a strengthening of the dense Arctic overturning between 1993–2020. This strengthening corresponds to sea-ice loss and increased surface transformation in the Barents Sea and north of Svalbard. However, as demonstrated in this study, transformed waters are not exported directly from these regions but generally flow cyclonically around the Arctic Ocean before being exported to the Nordic Seas through Fram Strait. Consistent with tracer studies (Wefing et al., 2021; Pasqualini et al., 2024), we find that the mean transit time of intermediate depth Atlantic Water through the Eurasian Basin back to Fram Strait is 10–20 years (Fig. 7). If the anomalous water masses formed by increased surface forcing in the Arctic Ocean during recent decades have mainly followed this Eurasian Basin pathway,

this would thus be reflected in a strengthened overturning circulation (i.e. increased export of dense waters rather than local storage; Buckley et al., 2023). A more detailed analysis of recent changes in the Arctic overturning circulation will be the topic of another study.

In this study, we have focused on annually averaged water mass transformations and overturning. There is additionally large seasonality in the mechanisms of overturning, especially in the surface forcing (Fig. 11, Pemberton et al., 2015). In winter, surface forcing produces both cooled and densified Atlantic Water from the Barents Sea and dense, brine-enriched waters near the freezing point from sea ice formation. These are subsequently homogenized through mixing into dense shelf waters. Approximately opposite transformations occur in the summer months. In the annual average, however, these dense shelf waters are essential for densifying Fram Strait Branch waters to outflow densities (Fig. 5b). Notably, the Barents Sea Branch experiences stronger freshening from mixing during winter than summer, despite the greater availability of freshwater in summer. This is likely due to weaker stratification in winter, which allows wind-driven mixing and cooling-induced deepening of the mixed layer to mix freshwater down into the Atlantic Water layer. The convergence of outflow waters, both recirculated Fram Strait Atlantic Water and the densest components of the outflow (Figs. 4 and 5b), show minimal seasonal variability. Finally, the estuarine cell's seasonal variability is set by fresh-

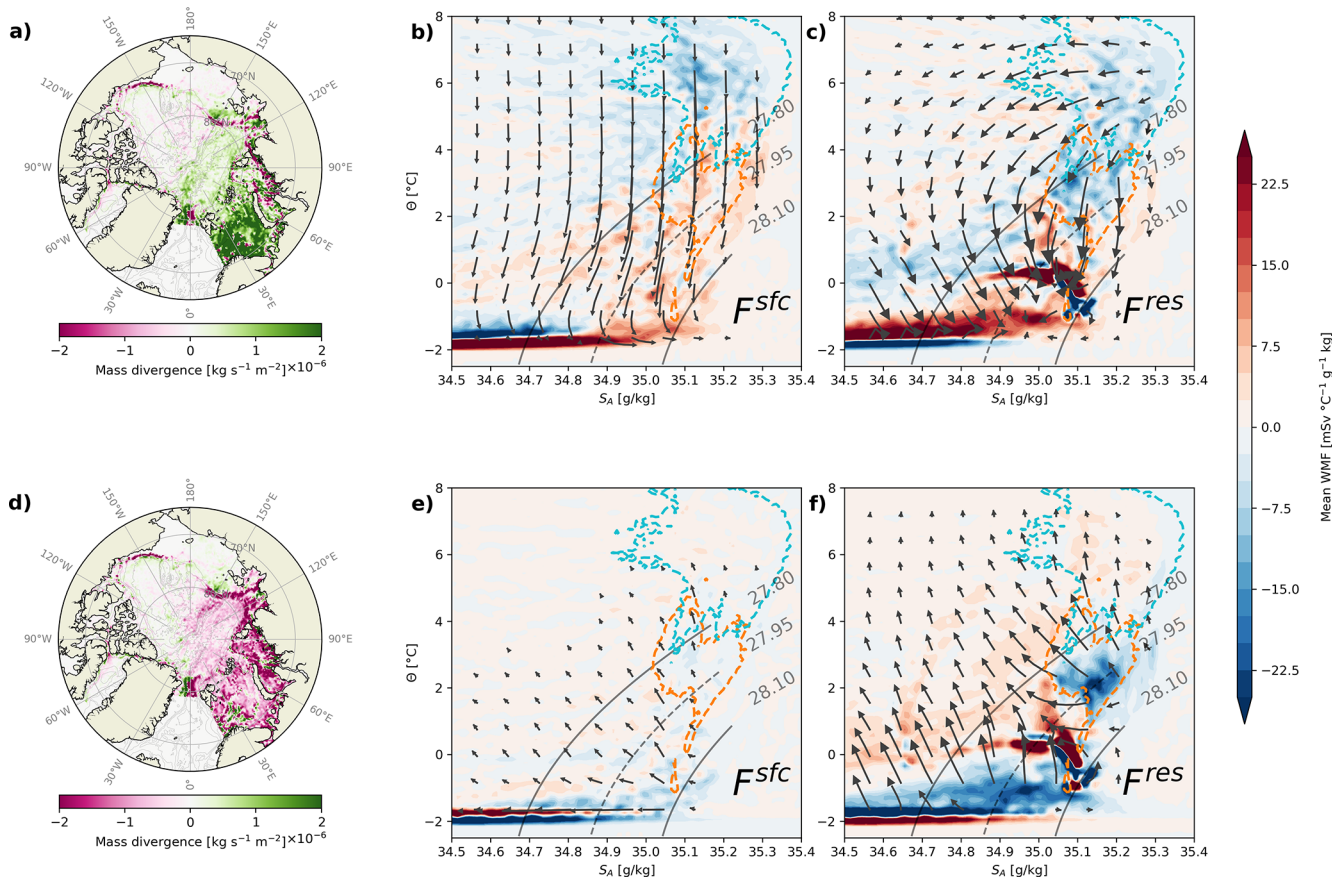


Figure 11. Seasonality of Arctic water mass transformation. Total water mass transformation during winter (October–March, **a–c**) and summer (April–September, **d–f**) from Lagrangian (**a, d**) and Eulerian (**b, c, e, f**) perspectives. (**a, d**) as Fig. 9a and b, but for all trajectories started at Fram Strait and the Barents Sea Opening, and for winter and summer, respectively. (**b, c**) as Fig. 5, but for winter. (**e, f**) as Fig. 5, but for summer.

water mixing along the Siberian Coast, which is stronger in summer.

Our study presents, for the first time, a comprehensive analysis of the hydrographic and spatial structure of the Arctic overturning circulation based on the period 1979–2015. During this period the Arctic Ocean experienced large changes in e.g. sea ice extent and hydrography (Stroeve and Notz, 2018; Polyakov et al., 2017), and further warming and sea ice loss are expected (Årthun et al., 2019; Notz and SIMIP community, 2020; Dörr et al., 2024). Our results can thus be used as a baseline when analyzing and interpreting recent and future changes in the Arctic overturning circulation and their causes and impacts.

Appendix A

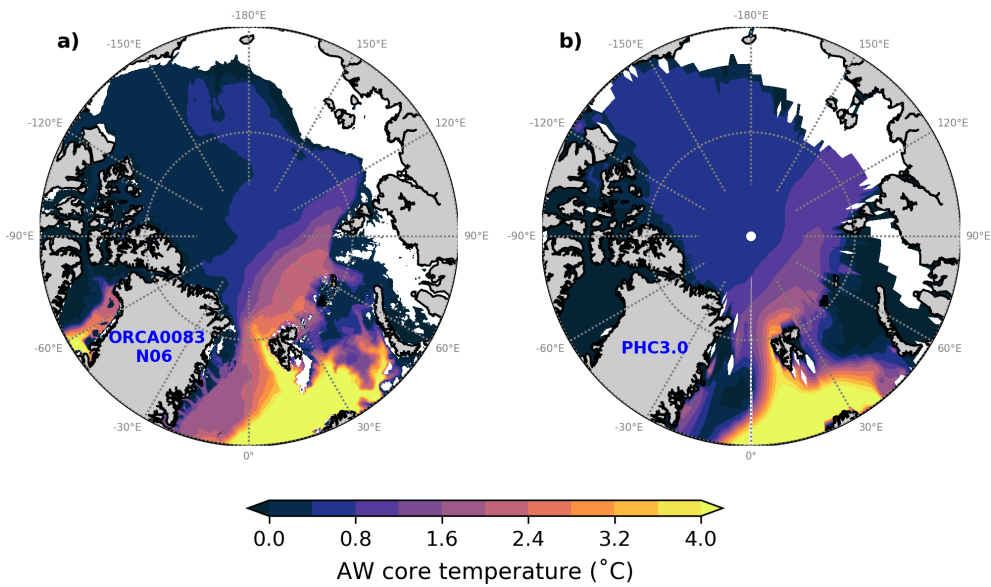


Figure A1. Comparison of the Atlantic Water core temperature in (a) ORCA0083-N06 (1979–2015) and (b) PHC3.0 (based on data from 1950–2005; Steele et al., 2001). The core temperature is the maximum temperature of the water column where the salinity is above 34.7. Shelf regions with a depth lower than 100 m are not shown.

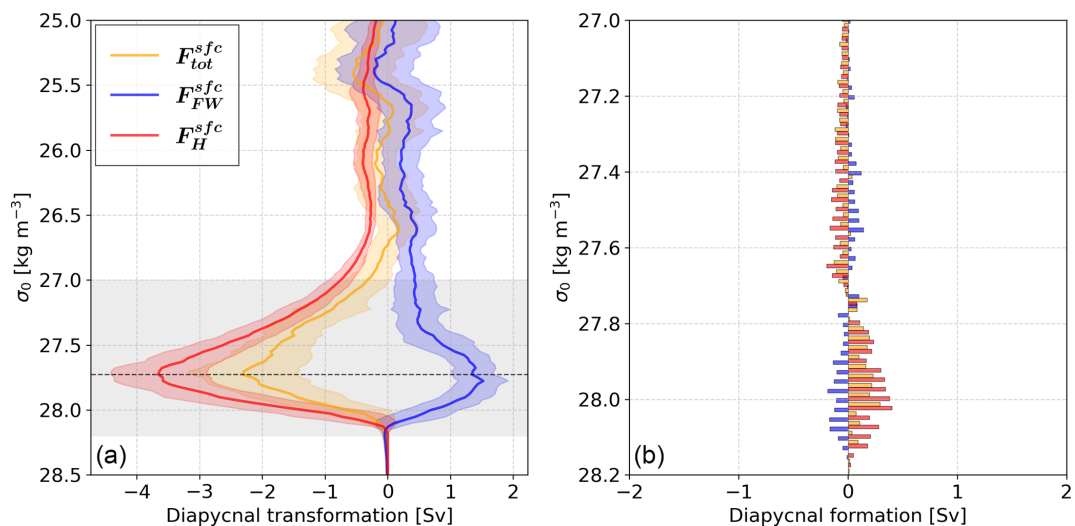


Figure A2. Time-mean diapycnal surface forced water mass transformation (a) and formation (b) for the Arctic Ocean from 1979–2015. The respective colors represent the total surface forced transformation (yellow), the freshwater component of the surface forced transformation (blue), and the heat component of the surface forced transformation (red), as well as their yearly standard deviation in shading. The individual heat and freshwater components are obtained by computing the transformation with the other surface flux set to zero. The quantities in (b) are calculated as the divergence of those in (a). The gray shading in (a) represents the extent of the y axis in (b).

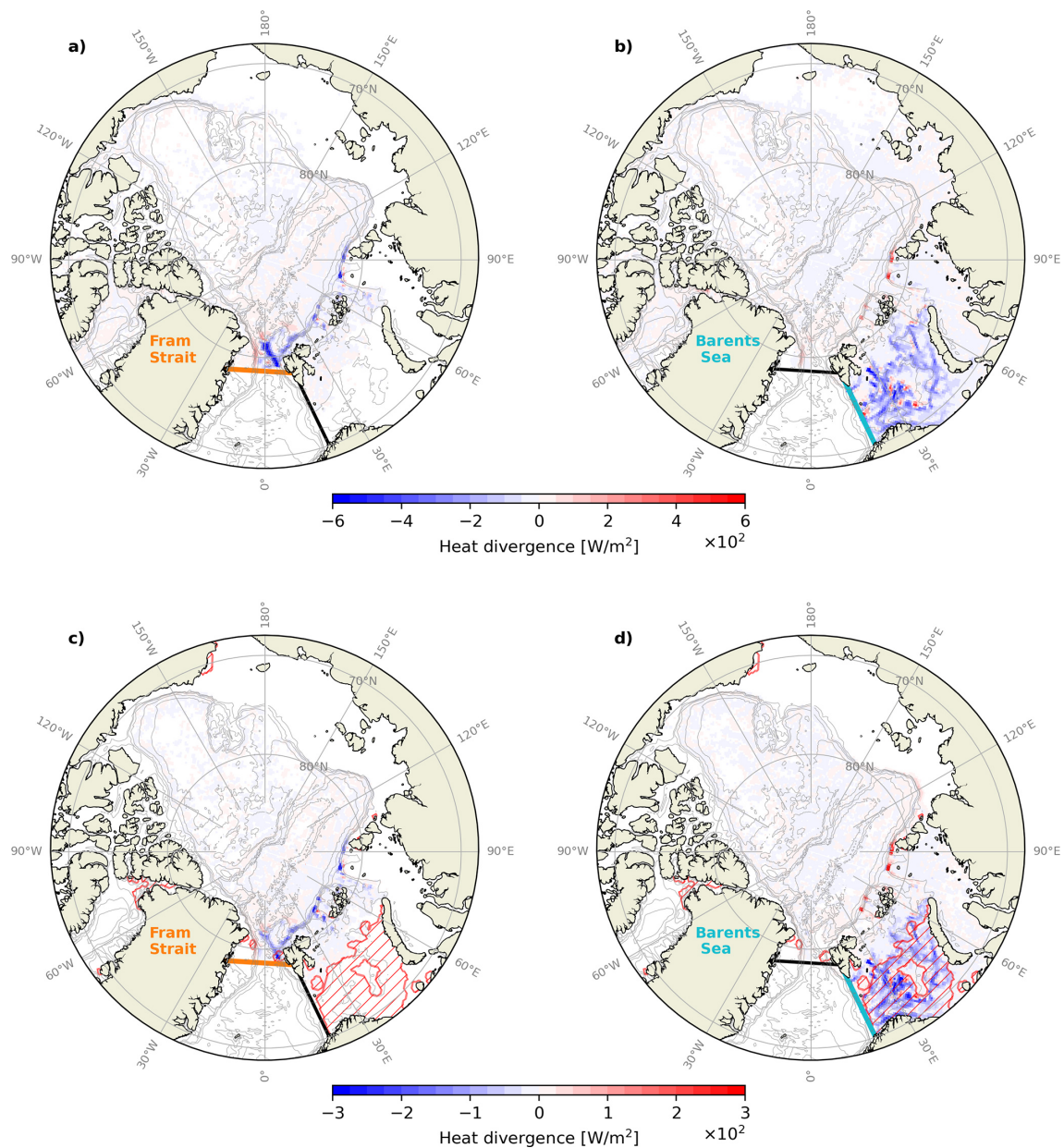


Figure A3. As Fig. 9, but for heat divergence.

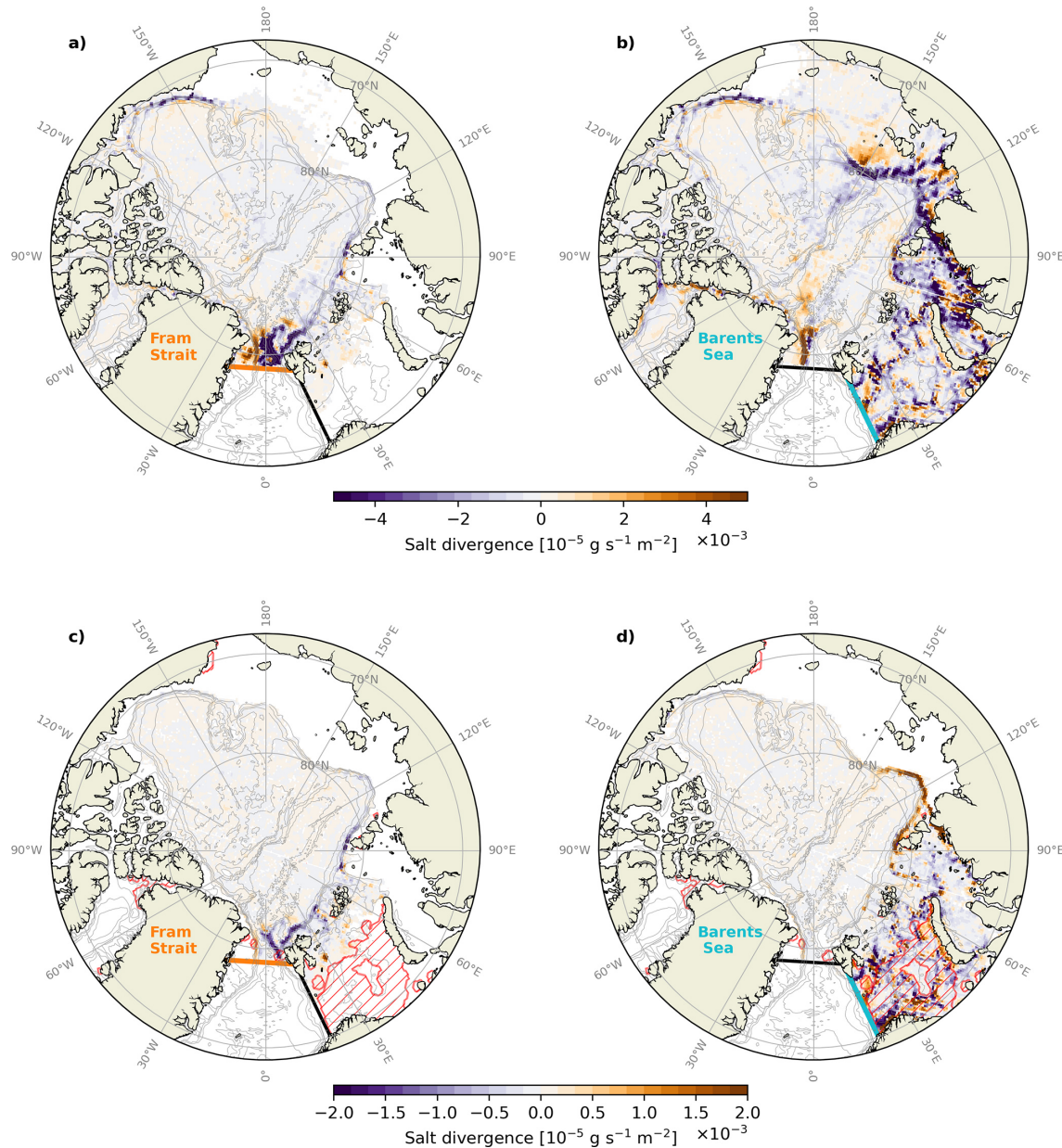


Figure A4. As Fig. 9, but for salt divergence.

Code and data availability. Monthly output from the ORCA0083-N06 hindcast can be found at <https://gws-access.jasmin.ac.uk/public/nemo/runs/ORCA0083-N06/means/> (last access: 26 March 2025). The source code of TRACMASS version 7.0 is available from <https://doi.org/10.5281/zenodo.4337926> (Aldama-Campino et al., 2020). The code for the Water Mass Transformation analysis is available from <https://github.com/dgwynevans/wmt> (Evans, 2023). The PHC3.0 climatology is available from <https://odv.awi.de/data/ocean/phc-30/> (last access: 2 June 2025). Lagrangian trajectory data produced in this study can be found at <https://doi.org/10.5281/zenodo.17047094> (Dörr, 2025).

Author contributions. JD, CM and MÅ conceived the study. MÅ acquired the funding for this study. JD and CM carried out all analysis and prepared the original draft. All authors interpreted the results, and reviewed and edited the final version of the manuscript.

Competing interests. The contact author has declared that none of the authors has any competing interests.

Disclaimer. Publisher's note: Copernicus Publications remains neutral with regard to jurisdictional claims made in the text, published maps, institutional affiliations, or any other geographical representation in this paper. The authors bear the ultimate responsibility for providing appropriate place names. Views expressed in the text are those of the authors and do not necessarily reflect the views of the publisher.

Acknowledgements. This work was funded by the Research Council of Norway project Overturning circulation in the new Arctic (Grant 335255). We thank two anonymous reviewers for providing helpful comments that improved the quality of this study.

Financial support. This research has been supported by the Norges Forskningsråd (grant no. 335255).

Review statement. This paper was edited by Sjoerd Groeskamp and reviewed by two anonymous referees.

References

Aagaard, K., Coachman, L. K., and Carmack, E.: On the halocline of the Arctic Ocean, *Deep-Sea Res.*, 28, 529–545, [https://doi.org/10.1016/0198-0149\(81\)90115-1](https://doi.org/10.1016/0198-0149(81)90115-1), 1981.

Aksenov, Y., Ivanov, V. V., Nurser, A. J. G., Bacon, S., Polyakov, I. V., Coward, A. C., Naveira-Garabato, A. C., and Beszczynska-Möller, A.: The Arctic circum-polar boundary current, *J. Geophys. Res.-Oceans*, 116, <https://doi.org/10.1029/2010JC006637>, 2011.

Aldama-Campino, A., Döös, K., Kjellsson, J., and Jönsson, B.: TRACMASS: Formal release of version 7.0, Zenodo [code], <https://doi.org/10.5281/zenodo.4337926>, 2020.

Årthun, M.: Surface-forced variability in the Nordic Seas overturning circulation and overflows, *Geophys. Res. Lett.*, 50, e2023GL104158, <https://doi.org/10.1029/2023GL104158>, 2023.

Årthun, M., Ingvaldsen, R., Smedsrød, L., and Schrum, C.: Dense water formation and circulation in the Barents Sea, *Deep-Sea Res.*, 58, 801–817, <https://doi.org/10.1016/j.dsr.2011.06.001>, 2011.

Årthun, M., Eldevik, T., and Smedsrød, L. H.: The role of Atlantic heat transport in future Arctic winter sea ice loss, *J. Climate*, 32, 3327–3341, <https://doi.org/10.1175/JCLI-D-18-0750.1>, 2019.

Årthun, M., Brakstad, A., Dörr, J., Johnson, H. L., Mans, C., Semper, S., and Våge, K.: Atlantification drives recent strengthening of the Arctic overturning circulation, *Science Advances*, 11, eadu1794, <https://doi.org/10.1126/sciadv.adu1794>, 2025.

Asbjørnsen, H. and Årthun, M.: Deconstructing future AMOC decline at 26.5°N, *Geophys. Res. Lett.*, 50, e2023GL103515, <https://doi.org/10.1029/2023GL103515>, 2023.

Athanase, M., Provost, C., Pérez-Hernández, M. D., Sennéchal, N., Bertosio, C., Artana, C., Garric, G., and Lellouche, J.-M.: Atlantic water modification north of Svalbard in the Mercator physical system from 2007 to 2020, *J. Geophys. Res.-Oceans*, 125, e2020JC016463, <https://doi.org/10.1029/2020JC016463>, 2020.

Bacon, S., Garabato, A. C. N., Aksenov, Y., Brown, N. J., and Tsubouchi, T.: Arctic Ocean boundary exchanges: a review, *Oceanography*, 35, 94–102, <https://doi.org/10.5670/oceanog.2022.133>, 2022.

Berglund, S., Döös, K., and Nycander, J.: Lagrangian tracing of the water–mass transformations in the Atlantic Ocean, *Tellus A*, 69, 1306311, <https://doi.org/10.1080/16000870.2017.1306311>, 2017.

Berglund, S., Döös, K., Groeskamp, S., and McDougall, T.: North Atlantic ocean circulation and related exchange of heat and salt between water masses, *Geophys. Res. Lett.*, 50, e2022GL100989, <https://doi.org/10.1029/2022GL100989>, 2023.

Beszczynska-Möller, A., Woodgate, R., Lee, C., Melling, H., and Kärcher, M.: A synthesis of exchanges through the main oceanic gateways to the Arctic Ocean, *Oceanography*, 24, 82–99, <https://doi.org/10.5670/oceanog.2011.59>, 2011.

Beszczynska-Möller, A., Fahrbach, E., Schauer, U., and Hansen, E.: Variability in Atlantic water temperature and transport at the entrance to the Arctic Ocean, 1997–2010, *ICES J. Mar. Sci.*, 69, 852–863, <https://doi.org/10.1093/icesjms/fss056>, 2012.

Bretones, A., Nisancioglu, K. H., Jensen, M. F., Brakstad, A., and Yang, S.: Transient increase in Arctic deep-water formation and ocean circulation under sea-ice retreat, *J. Climate*, 35, 109–124, 2022.

Brown, N. J., Naveira Garabato, A. C., Bacon, S., Aksenov, Y., Tsubouchi, T., Green, M., Lincoln, B., Rippeth, T., and Feltham, D. L.: The Arctic Ocean double estuary: quantification and forcing mechanisms, *AGU Advances*, 6, e2024AV001529, <https://doi.org/10.1029/2024AV001529>, 2025.

Buckley, M. W., Lozier, M. S., Desbruyères, D., and Evans, D. G.: Buoyancy forcing and the subpolar Atlantic meridional overturning circulation, *Philos. T. Roy. Soc. A*, 381, 20220181, <https://doi.org/10.1098/rsta.2022.0181>, 2023.

Carmack, E. and Wassmann, P.: Food webs and physical–biological coupling on pan-Arctic shelves: unifying concepts and comprehensive perspectives, *Prog. Oceanogr.*, 71, 446–477, <https://doi.org/10.1016/j.pocean.2006.10.004>, 2006.

Chafik, L. and Rossby, T.: Volume, heat, and freshwater divergences in the subpolar North Atlantic suggest the Nordic Seas as key to the state of the meridional overturning circulation, *Geophys. Res. Lett.*, 46, 4799–4808, 2019.

Coachman, L. and Barnes, C.: The movement of Atlantic water in the Arctic Ocean, *Arctic*, 16, 8–16, 1963.

Cornish, S. B., Johnson, H. L., Mallett, R. D. C., Dörr, J., Kostov, Y., and Richards, A. E.: Rise and fall of sea ice production in the Arctic Ocean's ice factories, *Nat. Commun.*, 13, 7800, <https://doi.org/10.1038/s41467-022-34785-6>, 2022.

Cottier, F. R. and Venables, E. J.: On the double-diffusive and cabbeling environment of the Arctic Front, West Spitsbergen, *Polar Res.*, 26, 152–159, <https://doi.org/10.1111/j.1751-8369.2007.00024.x>, 2007.

Curry, B., Lee, C. M., and Petrie, B.: Volume, freshwater, and heat fluxes through Davis Strait, 2004–05, *J. Phys. Oceanogr.*, 41, 429–436, <https://doi.org/10.1175/2010JPO4536.1>, 2011.

Dey, D., Marsh, R., Drijfhout, S., Josey, S. A., Sinha, B., Grist, J., and Döös, K.: Formation of the Atlantic Meridional Overturning Circulation lower limb is critically dependent on Atlantic–Arctic mixing, *Nat. Commun.*, 15, 7341, <https://doi.org/10.1038/s41467-024-51777-w>, 2024.

Dickson, R. R. and Brown, J.: The production of North Atlantic Deep Water: sources, rates, and pathways, *J. Geophys. Res.-Oceans*, 99, 12319–12341, 1994.

Dörr, J.: Lagrangian trajectory data in the Arctic Ocean, Zenodo [data set], <https://doi.org/10.5281/zenodo.17047094>, 2025.

Dörr, J., Årthun, M., Eldevik, T., and Sandø, A. B.: Expanding influence of Atlantic and Pacific Ocean heat transport on winter sea-ice variability in a warming Arctic, *J. Geophys. Res.-Oceans*, 129, e2023JC019900, <https://doi.org/10.1029/2023JC019900>, 2024.

Döös, K., Jönsson, B., and Kjellsson, J.: Evaluation of oceanic and atmospheric trajectory schemes in the TRACMASS trajectory model v6.0, *Geosci. Model Dev.*, 10, 1733–1749, <https://doi.org/10.5194/gmd-10-1733-2017>, 2017.

Dussin, R., Barnier, B., Brodeau, L., and Molines, J. M.: The Making of the Drakkar Forcing Set DFS5, Zenodo, <https://doi.org/10.5281/zenodo.1209243>, 2018.

Eldevik, T. and Nilsen, J. E. Ø.: The Arctic–Atlantic Thermohaline Circulation, *J. Climate*, 26, 8698–8705, <https://doi.org/10.1175/JCLI-D-13-00305.1>, 2013.

Evans, D. G.: Code for Water Mass Transformation Analysis, Github [code], <https://github.com/dgwynevans/wmt> (last access: 1 June 2024), 2023.

Evans, D. G., Zika, J. D., Naveira Garabato, A. C., and Nurser, A. J. G.: The imprint of Southern Ocean overturning on seasonal water mass variability in Drake Passage, *J. Geophys. Res.-Oceans*, 119, 7987–8010, <https://doi.org/10.1002/2014JC010097>, 2014.

Evans, D. G., Holliday, N. P., Bacon, S., and Le Bras, I.: Mixing and air–sea buoyancy fluxes set the time-mean overturning circulation in the subpolar North Atlantic and Nordic Seas, *Ocean Sci.*, 19, 745–768, <https://doi.org/10.5194/os-19-745-2023>, 2023.

Fer, I., Müller, M., and Peterson, A. K.: Tidal forcing, energetics, and mixing near the Yermak Plateau, *Ocean Sci.*, 11, 287–304, <https://doi.org/10.5194/os-11-287-2015>, 2015.

Groeskamp, S., Griffies, S. M., Iudicone, D., Marsh, R., Nurser, A. G., and Zika, J. D.: The water mass transformation framework for ocean physics and biogeochemistry, *Annu. Rev. Mar. Sci.*, 11, 271–305, <https://doi.org/10.1146/annurev-marine-010318-095421>, 2019.

Haine, T. W.: A conceptual model of polar overturning circulations, *J. Phys. Oceanogr.*, 51, 727–744, 2021.

Hieronymus, M., Nilsson, J., and Nycander, J.: Water mass transformation in salinity–temperature space, *J. Phys. Oceanogr.*, 44, 2547–2568, <https://doi.org/10.1175/JPO-D-13-0257.1>, 2014.

Ivanov, V. V., Danshina, A. V., Smirnov, A. V., and Filchuk, K. V.: Transformation of the atlantic water between svalbard and Franz Joseph Land in the late winter 2018–2019, *Deep-Sea Res. Pt. I*, 206, 104280, <https://doi.org/10.1016/j.dsr.2024.104280>, 2024.

Janout, M. A. and Lenn, Y.-D.: Semidiurnal tides on the Laptev Sea Shelf with implications for shear and vertical mixing, *J. Phys. Oceanogr.*, 44, 202–219, <https://doi.org/10.1175/JPO-D-12-0240.1>, 2014.

Janout, M. A., Hölemann, J., Timokhov, L., Gutjahr, O., and Heinemann, G.: Circulation in the northwest Laptev Sea in the eastern Arctic Ocean: crossroads between Siberian River water, Atlantic water and polynya-formed dense water, *J. Geophys. Res.-Oceans*, 122, 6630–6647, <https://doi.org/10.1002/2017JC013159>, 2017.

Karam, S., Heuzé, C., Hoppmann, M., and de Steur, L.: Continued warming of deep waters in the Fram Strait, *Ocean Sci.*, 20, 917–930, <https://doi.org/10.5194/os-20-917-2024>, 2024.

Kelly, S., Popova, E., Aksenov, Y., Marsh, R., and Yool, A.: Lagrangian modeling of Arctic Ocean circulation pathways: impact of advection on spread of pollutants, *J. Geophys. Res.-Oceans*, 123, 2882–2902, <https://doi.org/10.1002/2017JC013460>, 2018.

Kelly, S. J., Proshutinsky, A., Popova, E. K., Aksenov, Y. K., and Yool, A.: On the origin of water masses in the Beaufort Gyre, *J. Geophys. Res.-Oceans*, 124, 4696–4709, <https://doi.org/10.1029/2019JC015022>, 2019.

Lique, C. and Thomas, M. D.: Latitudinal shift of the Atlantic Meridional Overturning Circulation source regions under a warming climate, *Nat. Clim. Change*, 8, 1013–1020, 2018.

Lique, C., Treguier, A. M., Blanke, B., and Grima, N.: On the origins of water masses exported along both sides of Greenland: a Lagrangian model analysis, *J. Geophys. Res.-Oceans*, 115, <https://doi.org/10.1029/2009JC005316>, 2010.

Moat, B. I., Josey, S. A., and Sinha, B.: Impact of Barents Sea winter air-sea exchanges on Fram Strait dense water transport, *J. Geophys. Res.-Oceans*, 119, 1009–1021, <https://doi.org/10.1002/2013JC009220>, 2014.

Moat, B. I., Josey, S. A., Sinha, B., Blaker, A. T., Smeed, D. A., McCarthy, G. D., Johns, W. E., Hirschi, J. J.-M., Frajka-Williams, E., Rayner, D., Ducez, A., and Coward, A. C.: Major variations in subtropical North Atlantic heat transport at short (5 day) timescales and their causes, *J. Geophys. Res.-Oceans*, 121, 3237–3249, <https://doi.org/10.1002/2016JC011660>, 2016.

Notz, D. and SIMIP community: Arctic sea ice in CMIP6, *Geophys. Res. Lett.*, 47, e2019GL086749, <https://doi.org/10.1029/2019GL086749>, 2020.

Nurser, A. J. G. and Griffies, S. M.: Relating the diffusive salt flux just below the ocean surface to boundary freshwater and salt fluxes, *J. Phys. Oceanogr.*, <https://doi.org/10.1175/JPO-D-19-0037.1>, 2019.

Orvik, K. A. and Niiler, P.: Major pathways of Atlantic water in the northern North Atlantic and Nordic Seas toward Arctic, *Geophys. Res. Lett.*, 29, 2–1, 2002.

Pasqualini, A., Schlosser, P., Newton, R., Smethie Jr., W. M., and Friedrich, R.: A multi-decade tracer study of the circulation and spreading rates of Atlantic water in the Arctic Ocean, *J. Geophys. Res.-Oceans*, 129, e2023JC020738, <https://doi.org/10.1029/2023JC020738>, 2024.

Pemberton, P., Nilsson, J., Hieronymus, M., and Meier, H. E. M.: Arctic ocean water mass transformation in *S*–*T* coordinates, *J. Phys. Oceanogr.*, 45, 1025–1050, <https://doi.org/10.1175/JPO-D-14-0197.1>, 2015.

Petit, T., Lozier, M. S., Josey, S. A., and Cunningham, S. A.: Atlantic deep water formation occurs primarily in the Iceland Basin and Irminger Sea by local buoyancy forcing, *Geophys. Res. Lett.*, 47, e2020GL091028, <https://doi.org/10.1029/2020GL091028>, 2020.

Polyakov, I., Pnyushkov, A. V., Alkire, M. B., Ashik, I. M., Baumann, T. M., Carmack, E. C., Gosczko, I., Guthrie, J., Ivanov, V. V., Kanzow, T., Krishfield, R., Kwok, R., Sundfjord, A., Morison, J., Rember, R., and Yulin, A.: Greater role for Atlantic inflows on sea-ice loss in the Eurasian Basin of the Arctic Ocean, *Science*, 356, 285–291, <https://doi.org/10.1126/science.aai8204>, 2017.

Renner, A. H. H., Sundfjord, A., Janout, M. A., Ingvaldsen, R. B., Beszczynska-Möller, A., Pickart, R. S., and Pérez-Hernández, M. D.: Variability and redistribution of heat in the Atlantic water boundary current north of Svalbard, *J. Geophys. Res.-Oceans*, 123, 6373–6391, <https://doi.org/10.1029/2018JC013814>, 2018.

Rippeth, T. P., Lincoln, B. J., Lenn, Y.-D., Green, J. A. M., Sundfjord, A., and Bacon, S.: Tide-mediated warming of Arctic halocline by Atlantic heat fluxes over rough topography, *Nat. Geosci.*, 8, 191–194, <https://doi.org/10.1038/ngeo2350>, 2015.

Rudels, B. and Carmack, E.: Arctic Ocean water mass structure and circulation, *Oceanography*, 35, 52–65, 2022.

Rudels, B., Jones, E. P., Schauer, U., and Eriksson, P.: Atlantic sources of the Arctic Ocean surface and halocline waters, *Polar Res.*, 23, 181–208, 2004.

Rudels, B., Korhonen, M., Schauer, U., Pisarev, S., Rabe, B., and Wisotzki, A.: Circulation and transformation of Atlantic water in the Eurasian Basin and the contribution of the fram strait inflow branch to the Arctic Ocean heat budget, *Prog. Oceanogr.*, 132, 128–152, <https://doi.org/10.1016/j.pocean.2014.04.003>, 2015.

Saloranta, T. M., and Haugan, P. M.: Northward cooling and freshening of the warm core of the West Spitsbergen Current, *Polar Res.*, 23, 79–88, <https://doi.org/10.3402/polar.v23i1.6268>, 2004.

Schauer, U., Rudels, B., Jones, E. P., Anderson, L. G., Muench, R. D., Björk, G., Swift, J. H., Ivanov, V., and Larsson, A.-M.: Confluence and redistribution of Atlantic water in the Nansen, Amundsen and Makarov basins, *Ann. Geophys.*, 20, 257–273, <https://doi.org/10.5194/angeo-20-257-2002>, 2002.

Skagseth, Ø., Eldevik, T., Årthun, M., Asbjørnsen, H., Lien, V. S., and Smedsrød, L. H.: Reduced efficiency of the Barents Sea cooling machine, *Nat. Clim. Chang.*, 10, 661–666, <https://doi.org/10.1038/s41558-020-0772-6>, 2020.

Smedsrød, L. H., Esau, I., Ingvaldsen, R. B., Eldevik, T., Haugan, P. M., Li, C., Lien, V. S., Olsen, A., Omar, A. M., Otterå, O. H., Risebrobakken, B., Sandø, A. B., Semenov, V. A., and Sorokina, S. A.: The role of the Barents Sea in the Arctic climate system, *Rev. Geophys.*, 51, 415–449, <https://doi.org/10.1002/rog.20017>, 2013.

Smedsrød, L. H., Muilwijk, M., Brakstad, A., Madonna, E., Lauvset, S. K., Spensberger, C., Born, A., Eldevik, T., Drange, H., Jeansson, E., Li, C., Olsen, A., Skagseth, Ø., Slater, D. A., Straneo, F., Våge, K., and Årthun, M.: Nordic seas heat loss, Atlantic inflow, and Arctic sea ice cover over the last century, *Rev. Geophys.*, 60, e2020RG000725, <https://doi.org/10.1029/2020RG000725>, 2022.

Steele, M., Morley, R., and Ermold, W.: PHC: a global ocean hydrography with a high-quality Arctic Ocean, *J. Climate*, 14, 2079–2087, [https://doi.org/10.1175/1520-0442\(2001\)014<2079:PAGOHW>2.0.CO;2](https://doi.org/10.1175/1520-0442(2001)014<2079:PAGOHW>2.0.CO;2), 2001.

Stroeve, J. and Notz, D.: Changing state of Arctic sea ice across all seasons, *Environ. Res. Lett.*, 13, 103001, <https://doi.org/10.1088/1748-9326/aade56>, 2018.

Timmermans, M.-L. and Marshall, J.: Understanding Arctic Ocean circulation: a review of ocean dynamics in a changing climate, *J. Geophys. Res.-Oceans*, 125, e2018JC014378, <https://doi.org/10.1029/2018JC014378>, 2020.

Tooth, O. J., Foukal, N. P., Johns, W. E., Johnson, H. L., and Wilson, C.: Lagrangian decomposition of the Atlantic Ocean heat transport at 26.5°N, *Geophys. Res. Lett.*, 51, e2023GL107399, <https://doi.org/10.1029/2023GL107399>, 2024.

Tsubouchi, T., von Appen, W.-J., Kanzow, T., and de Steur, L.: Temporal variability of the overturning circulation in the Arctic Ocean and the associated heat and freshwater transports during 2004–10, *J. Phys. Oceanogr.*, 54, 81–94, 2024.

Walin, G.: On the relation between sea-surface heat flow and thermal circulation in the ocean, *Tellus*, 34, 187–195, 1982.

Wefing, A.-M., Casacuberta, N., Christl, M., Gruber, N., and Smith, J. N.: Circulation timescales of Atlantic Water in the Arctic Ocean determined from anthropogenic radionuclides, *Ocean Sci.*, 17, 111–129, <https://doi.org/10.5194/os-17-111-2021>, 2021.

Weijer, W., Cheng, W., Garuba, O. A., Hu, A., and Nadiga, B. T.: CMIP6 models predict significant 21st century decline of the Atlantic meridional overturning circulation, *Geophys. Res. Lett.*, 47, e2019GL086075, <https://doi.org/10.1029/2019GL086075>, 2020.

Wilson, C., Aksenov, Y., Rynders, S., Kelly, S. J., Krumpen, T., and Coward, A. C.: Significant variability of structure and predictability of Arctic Ocean surface pathways affects basin-wide connectivity, *Communications Earth and Environment*, 2, 1–10, <https://doi.org/10.1038/s43247-021-00237-0>, 2021.

Woodgate, R. A.: Increases in the Pacific inflow to the Arctic from 1990 to 2015, and insights into seasonal trends and driving mechanisms from year-round Bering Strait mooring data, *Prog. Oceanogr.*, 160, 124–154, <https://doi.org/10.1016/j.pocean.2017.12.007>, 2018.

Yeager, S., Castruccio, F., Chang, P., Danabasoglu, G., Maroon, E., Small, J., Wang, H., Wu, L., and Zhang, S.: An outsized role for the Labrador Sea in the multidecadal variability of the Atlantic overturning circulation, *Science Advances*, 7, eabh3592, <https://doi.org/10.1126/sciadv.abh3592>, 2021.

Zhang, R. and Thomas, M.: Horizontal circulation across density surfaces contributes substantially to the long-term mean northern Atlantic Meridional Overturning Circulation, *Communications Earth and Environment*, 2, 1–12, <https://doi.org/10.1038/s43247-021-00182-y>, 2021.

Zou, S., Petit, T., Li, F., and Lozier, M. S.: Observation-based estimates of water mass transformation and formation in the Labrador Sea, *J. Phys. Oceanogr.*, <https://doi.org/10.1175/JPO-D-23-0235.1>, 2024.